Article

Cell Reports

Sumoylation of Smc5 Promotes Error-free Bypass at Damaged Replication Forks

Graphical Abstract

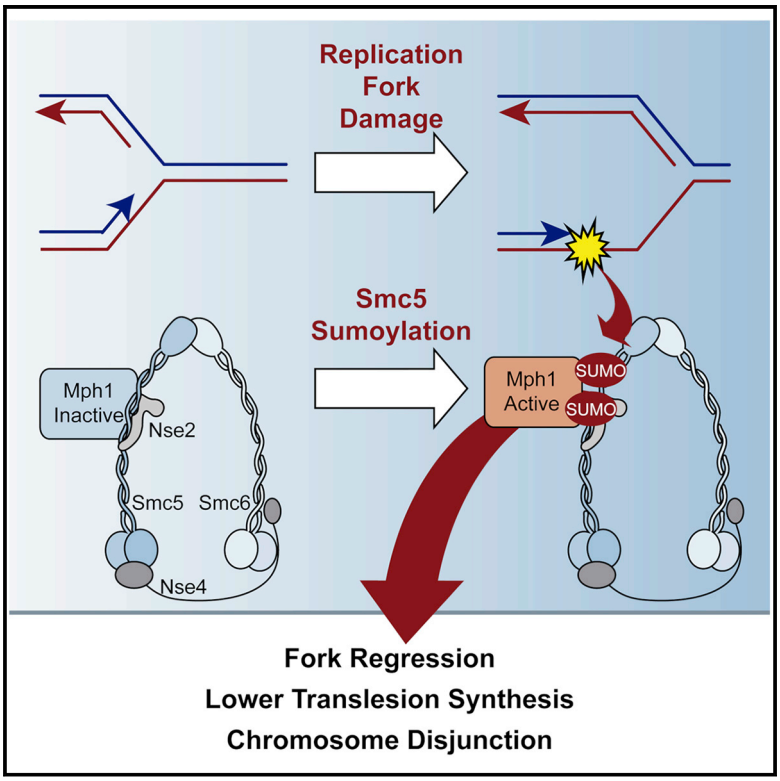

Highlights

- Smc5-SUMO is a specific read-out for damaged replication forks
- SUMO preferentially targets lysines in the coiled-coil domain of Smc5
- *smc5-KR* is epistatic to *MPH1*, upregulating TLS and reducing strand exchange
- Defects in Smc5 sumoylation are normally backed up by the Mms4-Mus81 nuclease

Authors

Mariel Zapatka, Irene Pociño-Merino, Hayat Heluani-Gahete, ..., Ralf Wellinger, Neus Colomina, Jordi Torres-Rosell

Correspondence

jordi.torres@cmb.udl.cat

In Brief

Zapatka et al. show that sumoylation of Smc5 helps cells tolerate DNA lesions at damaged replication forks in an error-free mode. Using unsumoylatable *smc5-KR* mutants, they show that this modification operates through Mph1 in fork regression, working in parallel with several nucleases and helicases to promote chromosome segregation.

Zapatka et al., 2019, Cell Reports *29*, 3160–3172
December 3, 2019
https://doi.org/10.1016/j.celrep.2019.10.123

CellPress

OPEN ACCESS
CellPress

Cell Reports
Article

Sumoylation of Smc5 Promotes Error-free Bypass at Damaged Replication Forks

Mariel Zapatka,[1,4] Irene Pociño-Merino,[1,4] Hayat Heluani-Gahete,[2] Marcelino Bermúdez-López,[1] Marc Tarrés,[1] Eva Ibars,[1] Roger Solé-Soler,[1] Pilar Gutiérrez-Escribano,[3] Sonia Apostolova,[1] Celia Casas,[1] Luis Aragon,[3] Ralf Wellinger,[2] Neus Colomina,[1] and Jordi Torres-Rosell[1,5,*]

[1]Departament de Ciencies Mediques Basiques, Institut de Recerca Biomedica de Lleida, Universitat de Lleida, 25198 Lleida, Spain
[2]CABIMER-Universidad de Sevilla, Avenida Americo Vespucio sn, 41092 Sevilla, Spain
[3]MRC London Institute of Medical Sciences, Du Cane Road, London W12 0NN, UK
[4]These authors contributed equally
[5]Lead Contact
*Correspondence: jordi.torres@cmb.udl.cat
https://doi.org/10.1016/j.celrep.2019.10.123

SUMMARY

Replication of a damaged DNA template can threaten the integrity of the genome, requiring the use of various mechanisms to tolerate DNA lesions. The Smc5/6 complex, together with the Nse2/Mms21 SUMO ligase, plays essential roles in genome stability through undefined tasks at damaged replication forks. Various subunits within the Smc5/6 complex are substrates of Nse2, but we currently do not know the role of these modifications. Here we show that sumoylation of Smc5 is targeted to its coiled-coil domain, is upregulated by replication fork damage, and participates in bypass of DNA lesions. *smc5-KR* mutant cells display defects in formation of sister chromatid junctions and higher translesion synthesis. Also, we provide evidence indicating that Smc5 sumoylation modulates Mph1-dependent fork regression, acting synergistically with other pathways to promote chromosome disjunction. We propose that sumoylation of Smc5 enhances physical remodeling of damaged forks, avoiding the use of a more mutagenic tolerance pathway.

INTRODUCTION

Accurate and complete DNA replication is a fundamental part of cell division. DNA replication forks are intrinsically fragile, and their stability can be further endangered by the presence of lesions in the template. DNA lesions can block or even collapse replication forks, leading to genomic instability and chromosomal rearrangements (Mizuno et al., 2013). Forks arrested by DNA damage accumulate single-stranded DNA (ssDNA) opposite the lesion, a signal that activates the DNA replication checkpoint (Zou and Elledge, 2003). The checkpoint then prevents cells to enter into mitosis and stabilizes replication forks until they are ready to restart, avoiding their collapse (Tercero and Diffley, 2001; Sogo et al., 2002). In parallel, activation of DNA damage tolerance (DDT) mechanisms allows cells to bypass the lesion, without the need to repair and incur into deleterious breaks, thereby enabling completion of DNA replication (Branzei and Psakhye, 2016; García-Rodríguez et al., 2016). DDT thus postpones DNA repair until the replication fork has moved away.

Most DDT mechanisms depend on modification of PCNA with ubiquitin and SUMO (Hoege et al., 2002). First, mono-ubiquitylation of PCNA at K164 leads to a switch from a high-fidelity replicative to a low-fidelity translesion synthesis (TLS) DNA polymerase (Lehmann et al., 2007). Although TLS polymerases are error prone, they can polymerase through lesions on the template. Second, K63-linked poly-ubiquitylation of PCNA at K164, leads to error-free recombination-based swapping of strands with the sister chromatid, a mechanism known as template switch (Branzei et al., 2008; Zhang and Lawrence, 2005). Swapping strands with the sister allows pairing the end blocked by a lesion with an undamaged template, facilitating resumption of replication. Third, homologous recombination can also be used independently from the template switch pathway at damaged replication forks (Papouli et al., 2005; Pfander et al., 2005). To prevent unscheduled recombination during S phase, which can promote genome rearrangements (Lambert and Carr, 2013), sumoylation of PCNA at either K164 or K127 normally recruits the anti-recombinase Srs2 helicase in budding yeast (Hoege et al., 2002; Papouli et al., 2005; Pfander et al., 2005). However, homologous recombination can still be invoked through Srs2 degradation as a salvage pathway to locally rescue stalled replication forks (Urulangodi et al., 2015). Both template switch and the salvage pathway ultimately generate sister chromatid junctions (SCJs), recombination structures that display exchange of strands between sister chromatids. Several DNA cleavage enzymes, including the Sgs1-Top3-Rmi1 (STR) complex, the Mms4-Mus81 complex, and the Slx4 and Yen1 nucleases, subsequently remove recombination intermediates. The STR complex is the major pathway for elimination of SCJs during S phase, while Mms4-Mus81 cleaves these structures in mitosis (Matos and West, 2014).

Whereas template switch can be spatially and temporally uncoupled from the replication fork (Daigaku et al., 2010; Karras and Jentsch, 2010), there is another DDT mechanism, able to anneal newly replicated strands specifically at the replication fork, in a process known as fork regression (Meng and

Zhao, 2017). This converts Y-shaped three-way junctions into four-way DNA structures. Replication fork regression protects damaged forks by preventing extensive ssDNA generation and by providing access of repair systems to the damaged template. Additionally, nucleolytic processing of regressed forks could potentially trigger invasion of parental strands ahead of the fork, generating SCJs (Meng and Zhao, 2017). There are several enzymes known to promote fork regression (Branzei and Szakal, 2017). Mph1 and its orthologs in human and fission yeast, FANCM and Fml1, are motor proteins able to catalyze remodeling of replication fork into regressed structures *in vitro* (Whitby, 2010). This activity allows Mph1 to function in template switch-independent error-free DNA damage bypass (Schürer et al., 2004). In accordance, Mph1-dependent recombination structures have been detected using two-dimensional (2D) gel electrophoresis in budding yeast (Chen et al., 2009; Choi et al., 2010; Chavez et al., 2011). *In vitro*, Mph1 function in fork regression, but not its D-loop disruptive activity, is counteracted by direct binding to the coiled-coil domain of the Smc5 protein (Xue et al., 2014). This function is assisted by the MHF complex, which helps overcome the inhibitory function of Smc5 on Mph1 (Xue et al., 2015).

Smc5 is one of the core subunits of the Smc5/6 complex, a member of the SMC family of protein complexes, with roles in chromosome segregation and DNA repair. SMC proteins are elongated molecules with one ATPase head at one end, separated by a long coiled coil from an heterodimerization or hinge domain at the other end. The Smc5/6 complex is composed of two SMC subunits (Smc5 and Smc6) and six non-SMC elements (Nse1–Nse6). Nse2 has an essential N-terminal domain that binds to the coiled-coil domain of Smc5 and a C-terminal domain coding for an SP-RING SUMO E3 ligase (Zhao and Blobel, 2005; Potts and Yu, 2005; Andrews et al., 2005). The activity of the Nse2 ligase is enhanced by ATPase-dependent loading of the complex onto chromatin and direct binding of DNA to the Smc5 molecule (Varejão et al., 2018; Bermúdez-López et al., 2015). Although the SP-RING domain is not essential for viability, its mutation reduces sumoylation of several chromosome associated proteins (Albuquerque et al., 2013) and results in DNA damage sensitivity. In accordance, two complexes directly involved in DNA repair, cohesin and STR, have been characterized as targets of Nse2 (Almedawar et al., 2012; Bermúdez-López et al., 2016; Bonner et al., 2016; McAleenan et al., 2012). In addition, the SP-RING domain promotes completion of DNA replication and chromosome segregation (Bermúdez-López et al., 2010, 2015), most probably by facilitating replication fork progression. This function is particularly critical in the rDNA array (Menolfi et al., 2015; Torres-Rosell et al., 2007). A recent study indicated that the Smc5/6-dependent inhibition of Mph1 fork regression activities in the rDNA array plays a prominent role in replication of this locus (Peng et al., 2018).

One of the most noticeable targets of the Nse2 SUMO ligase is its own docking site in the Smc5/6 complex, the Smc5 subunit (Bermúdez-López et al., 2016, 2015; Chen et al., 2009; Duan et al., 2009). However, we do not know the sites targeted by SUMO in the Smc5 protein, nor how it affects the function of the Smc5/6 complex in genome integrity. Here we map SUMO-targeted lysines to the coiled-coil domain of Smc5 and show that Smc5 is mainly sumoylated in response to replication fork damage. Furthermore, using SUMO-impaired *smc5-KR* mutants, we reveal that this modification promotes DDT though Mph1. In the absence of Smc5 sumoylation, cells upregulate mutagenic TLS and reduce the formation of SCJs. Finally, our results indicate that this lesion bypass mechanism is normally backed up by Mms4-Mus81, which allows the completion of chromosome replication and disjunction in the absence of Smc5 sumoylation.

RESULTS

Smc5 Is Specifically Sumoylated in Response to Replication Fork Damage in *S. cerevisiae*

Smc5 is the most highly sumoylated subunit of the Smc5/6 complex in *S. cerevisiae* (Bermúdez-López et al., 2016). Besides, sumoylation of Smc5 increases after exposure of cells to the alkylating agent methyl methanesulfonate (MMS), suggesting that this modification participates in repair of damaged replication forks. The Smc5/6 complex contributes to the repair not only of alkylation damage but also of a broad spectrum of genotoxic agents, including camptothecin (CPT), phleomycin, and hydroxyurea (HU) (Kegel and Sjögren, 2010). To better understand what induces Smc5 sumoylation, we treated yeast cells expressing Smc5-9xmyc and 6xhis-FLAG-Smt3 with various genotoxic agents. Protein extracts were prepared under strong denaturing conditions, and sumoylated proteins were purified using NiNTA affinity pull-downs. As shown in Figure 1A, Smc5 sumoylation is strongly induced by treatment with MMS. In contrast, it only shows residual activation by treatment with a lethal dose of phleomycin, and we did not detect any induction with HU or CPT. To ascertain the levels of DNA damage induced by each treatment, we analyzed phosphorylation of the Rad53 checkpoint kinase. MMS and phleomycin induced similar strong phosphorylation of Rad53, while HU and CPT induced a more modest response (Figure 1A). Therefore, although MMS induces a stronger sumoylation of Smc5 than phleomycin, the levels of checkpoint activity induced by both treatments are similar.

Next, we analyzed whether the specificity for MMS-induced damage is typical of all targets of the Nse2 SUMO ligase. To this end, we tested sumoylation of three additional Nse2 targets, Sgs1, Smc1, and Fob1. Sgs1 is the budding yeast homolog of the Bloom helicase, and its sumoylation is known to depend on Nse2 in yeast and human cells (Bermúdez-López et al., 2016; Bonner et al., 2016; Pond et al., 2019). Sgs1 sumoylation was almost undetectable in untreated cells and showed the highest induction in sumoylation after treatment with phleomycin, followed by MMS and CPT (Figure 1A). Smc1 is a subunit of the cohesin complex and its sumoylation also partly depends on Nse2 (McAleenan et al., 2012). Differently to Smc5 and Sgs1, Smc1 sumoylation was induced not only by MMS and phleomycin but also by HU and CPT (Figure 1A). The Fob1 protein binds to the repetitive rDNA locus throughout the cell cycle. Interestingly, Fob1 sumoylation is predominantly Nse2 dependent (Figure S1). Fob1 showed

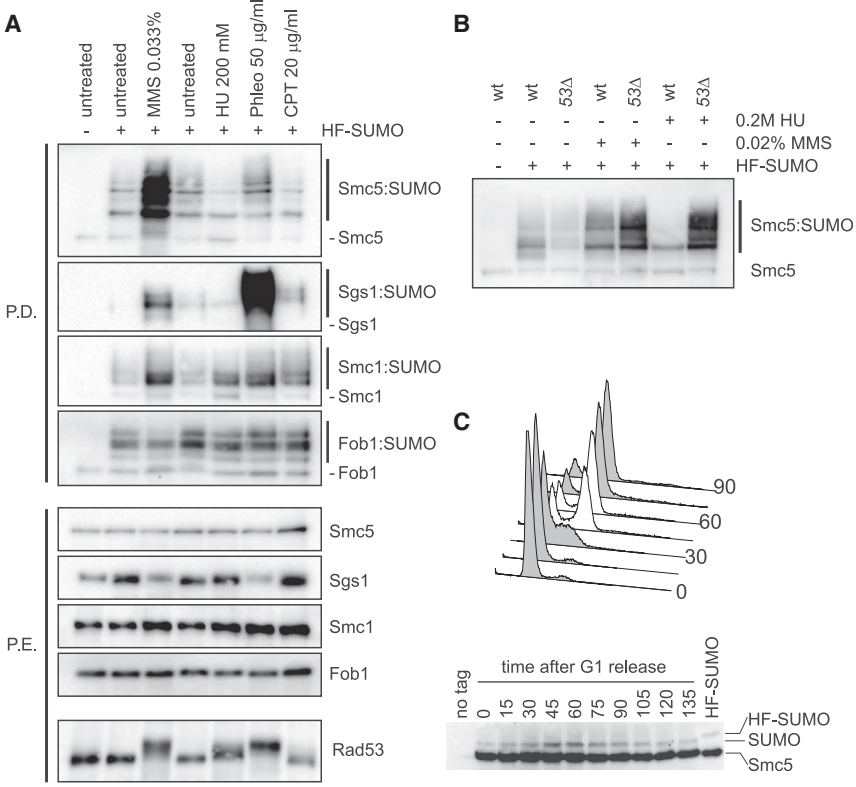

Figure 1. Sumoylation of Smc5 Is Specifically Induced in Response to Replication Fork Damage

(A) Pull-down analysis of Nse2 targets in response to genotoxic stress. Exponentially cells expressing 6xHis-FLAG (HF)-tagged SUMO and the indicated 6xHA-tagged Nse2 targets (Smc5, Sgs1, Smc1, and Fob1) were treated for 90 min with the indicated genotoxic agents. HF-SUMO was pulled down (P.D.) under denaturing conditions from yeast protein extracts (P.E.s) to purify sumoylated species. P.E. and P.D. samples were analyzed using western blot with the indicated antibodies. See also Figure S1.

(B) Wild-type (WT) and *rad53Δ slm1Δ* (*53Δ*) cells expressing HF-SUMO were treated with 0.02% MMS or 0.2 M HU. Samples were processed as in (A) to analyze sumoylation of Smc5.

(C) Cells expressing Smc5-9xmyc were arrested in G1 with alpha factor and were subsequently released into a synchronous cell cycle. Alpha factor was added again 45 min after release to prevent re-entry into a new cell cycle. Samples were taken for fluorescence-activated cell sorting (FACS) analysis (top panel) and anti-myc western blot (bottom panel). Smc5-SUMO species are detected as a band with lower electrophoretic mobility, and are shifted upward when SUMO carries the HF tag (last lane).

the least variation among the four tested Nse2 targets, with no particular induction by any of the DNA damaging agents tested (Figure 1A). Therefore, we conclude that not all Nse2 targets are sumoylated to the same extent by different types of DNA damage. In addition, our analysis reveals that Smc5 is specifically sumoylated in response to MMS.

Although both 0.033% MMS and 0.2 M HU severely affect replication fork progression and activate checkpoint responses in S phase, such as Rad53 phosphorylation, we noticed that treatment with HU actually reduced Smc5 sumoylation levels. This suggests that Smc5 is sumoylated in response not to replication fork arrest but to damaged replication forks. Replication forks arrested by dNTP depletion are stabilized by the DNA damage checkpoint, and inactivation of the Rad53 checkpoint kinase leads to replication fork collapse in response to HU-induced replicative stress (Lopes et al., 2001). As shown in Figure 1B, and differently from wild-type cells, *rad53Δ* mutant cells displayed a robust induction of Smc5 sumoylation in response to HU, suggesting that collapsed forks strongly promote Smc5 sumoylation. In addition, these results indicate that the DNA damage checkpoint does not participate in Smc5 sumoylation, as occurs with most other DNA damage-dependent SUMO targets (Cremona et al., 2012). Overall, we conclude that Smc5 sumoylation is upregulated in response to replication fork damage. In agreement, sumoylation of Smc5, detectable in total protein extracts as a band with lower electrophoretic mobility, peaks in middle-late S phase in cultures progressing synchronously from a G1 release (Figure 1C).

Identification of SUMO Acceptor Sites in Smc5 and Generation of a Non-sumoylatable Allele

We next set out to identify the sumoylated lysines in Smc5, using a mutational approach, with the aim to generate a non-sumoylatable *smc5* mutant. We started by changing all the lysines in the Smc5 protein (except K75 in the catalytic site) to arginines, thus generating an *smc5-KallR* allele. The mutant protein was expressed at similar levels to its wild-type counterpart but, as expected, was not sumoylated (Figure S2A). To identify regions in the Smc5 protein targeted by SUMO, we restrained *KR* mutations to specific domains in the Smc5 protein. We thus generated a set of five *smc5-KR* alleles, affected in each of these domains: *smc5-KR1* to *smc5-KR5* (Figure 2A). SUMO pull-down analysis showed that the sumoylation was slightly reduced in *smc5-KR3* cells, although the difference was not statistically significant (Holm-Bonferroni post hoc test), suggesting that sumoylation does not occur in the hinge domain (Figure 2B). In contrast, mutation of lysines in the head domains (*smc5-KR1* and *smc5-KR5*) diminished Smc5 sumoylation (Figure 2B). To test if the *KR* mutations affect SUMO ligase activity, we monitored sumoylation of the Smc6 subunit, which also depends on Nse2. As shown in Figure 2C, sumoylation of Smc6 was fully rescued by expression of *SMC5* in auxin-sensitive *smc5-aid* cells, but not by the *KallR* allele, and only partially by the *KR1* or *KR5* mutants. Therefore, the *smc5-KR1* and *smc5-KR5* sumoylation defects are most probably due not to mutation of SUMO acceptor sites but to lower Nse2 activity. As shown in Figure 2D, all *smc5-KR* alleles were viable, except *smc5-KallR*.

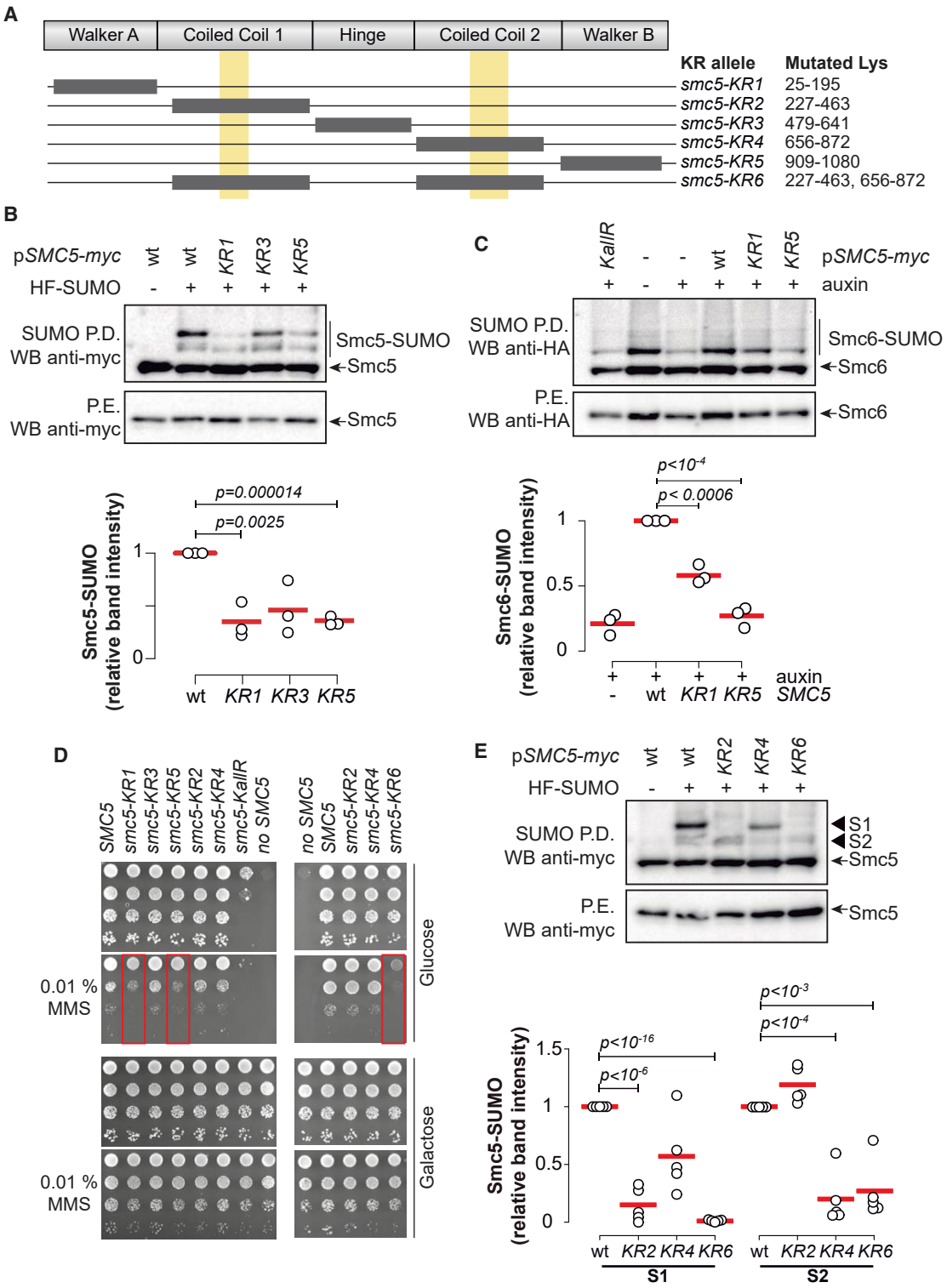

Figure 2. Identification of SUMO Acceptor Sites in Smc5

(A) Summary of the *KR* alleles generated, including affected domain/subdomain (in dark gray) and position of mutated residues. Yellow boxes indicate the Nse2-binding region in Smc5.

(B) Exponentially growing cultures of cells expressing *HF-SMT3* and the indicated *smc5-KR-9xmyc* mutants from centromeric vectors were collected and analyzed using pull-down of SUMO conjugates. Bottom panel: quantification of sumoylated Smc5 species from three independent pull-down experiments.

(legend continued on next page)

However, cells expressing the *smc5-KR1* and *smc5-KR5* mutants displayed sensitivity to MMS. Because most Smc5/6 mutants have reduced activity of the Nse2 ligase (Bermúdez-López et al., 2015), the most plausible explanation for the MMS sensitivity and lower Smc5 and Smc6 sumoylation is that *smc5-KR1* and *smc5-KR5* are hypomorphic for Smc5/6 and SUMO ligase function.

Interestingly, we observed that there were two main bands of Smc5 sumoylation in western blots, likely reflecting two different Smc5-SUMO species (S1 and S2; Figure 2E). The slowest migrating band (S1) most probably corresponds to modification of the first coiled-coil domain, as it was absent in a mutant smc5-KR2 protein (Figure 2E). In contrast, the lower band (S2) was specifically downregulated when lysine residues in coiled coil 2 were mutated (*smc5-KR4*), suggesting that this band mainly reports sumoylation of lysines in the second coiled coil (Figure 2E). The *smc5-KR2* and *smc5-KR4* mutants were able to complement the lack of expression of endogenous *SMC5* and displayed no growth defects in the presence of MMS (Figure 2D). Therefore, we reasoned that the altered sumoylation pattern of the *KR2* and *KR4* alleles is due to loss of acceptor SUMO sites. We conclude from these observations that lysines targeted by SUMO in the Smc5 protein are located in its coiled-coil domain. In accordance, SUMO pull-down experiments showed that an *smc5-KR6* allele, carrying mutations in all the lysines of the coiled coils, severely reduced Smc5 sumoylation (Figure 2E). However, the *smc5-KR6* allele also lowered Smc6-SUMO species (see below) and sensitized cells to MMS (Figure 2D). This could be due to a specific function of Smc5 sumoylation in response to MMS damage or, as observed in *smc5-KR1* or *smc5-KR5* mutants, to an hypomorphic phenotype in *smc5-KR6* cells.

Next, the coiled-coil domain of Smc5 was divided into three sub-sections, the hinge-proximal region, the Nse2 binding site, and the ATPase head-proximal region, to generate three new *KR* mutant alleles (Figure 3A). As shown in Figure 3B, sumoylation of Smc5 was not affected by mutation of lysines proximal to the ATPase head (*smc5-KR9*). In contrast, mutation of lysines proximal to the hinge domain (*smc5-KR7*) reduced S2 species, whereas mutation of lysines in the Nse2 binding site (*smc5-KR8*) diminished the intensity of the S1 band. These observations suggest that sumoylation occurs in the Nse2-binding region of the first coiled coil (between K310 and K356) and in the hinge-proximal region of the second coiled coil (between K656 and K745). To corroborate this prediction, we created a new allele that combined these two sets of *KR* mutations, *smc5-KR10*, which was severely impaired in sumoylation (Figure 3B). In response to 0.02% MMS treatment, *smc5-KR10* cells showed a specific reduction in the S1 band, indicating that K310 to K356 are also the main SUMO targets after replication fork damage (Figure S3). The presence of other sumoylated forms in *smc5-KR10* cells suggests that SUMO acceptor sites in Smc5 present some levels of redundancy, especially under conditions of extensive replication fork damage.

In an effort to further pinpoint the targeted lysines in Smc5, we generated a new allele, *smc5-KR11*, comprising the *KR* mutations closer to the boundary between the Nse2-binding site on coiled coil 1 and the hinge-proximal subdomain in coiled coil 2. However, these mutations did not alter the S1 sumoylation band (Figure 3B). This band seemed to depend on a group of lysines in the N-terminal side of the Nse2 binding site (K310–K337), as evidenced by the lack of the S1 band in the *smc5-KR12* allele (Figure 3B). To further identify the main sites of sumoylation in S1, we constructed a new allele, *smc5-KR13*, carrying mutations spanning K310–K327, which substantially reduced S1 sumoylation (Figure 3B). On the other hand, because both *smc5-KR11* and *smc5-KR12* showed somewhat reduced levels of the S2 band, but not as low as in the *smc5-KR10* allele (Figure 3B), we conclude that sumoylation in coiled coil 2 is quite dispersed. Overall, we propose that Smc5 has one major sumoylation hotspot, located between K310 and K327 in coiled coil 1; additionally, there is a second more diffuse sumoylation region in coiled coil 2, between K656 and K745. A summary of all the mutant alleles and their sumoylation levels is shown in Figure 3C. To verify that Smc5 can accept SUMO at these two locations, we sumoylated Smc5 in bacteria and analyzed the modified protein by mass spectrometry (Figures S3A–S3C). K311 and K667, which are located in the two regions mapped as SUMO acceptor sites in *smc5-KR10* cells, were identified as high-confidence sumoylated residues (Figures S3C and S3D). However, neither single nor double *K311R* and *K667R* mutants affected sumoylation of Smc5 *in vivo*, suggesting that Smc5 sumoylation sites are redundant (Figure S3E). The modification of other lysines *in vitro*, which were not identified using a *KR* mutagenesis strategy *in vivo*, may be due to the use of a human sumoylation machinery, in a bacterial environment, and in the absence of the rest of the Smc5/6 subunits.

The Nse2 SUMO Ligase Is Functional in an smc5-KR10 Mutant

Surprisingly, none of the *KR* mutants affected in the coiled-coil domain of Smc5 (except *smc5-KR6*) were sensitive to MMS (Figure 4A). Of note, the *smc5-KR10* allele, which shows very low levels of sumoylation, was wild-type for MMS sensitivity (Figures 3B and 4A). These results suggest that Smc5

(C) Exponentially growing cultures of *smc5-aid SMC6-6HA HF-SMT3* cells expressing the indicated *KR* alleles from a centromeric plasmid were treated with 1 mM IAA for 1 h, and samples were collected for SUMO pull-down analysis. Bottom panel: quantification of sumoylated Smc6 species from three independent pull-down experiments.
(D) Growth test analysis of *GAL1p-SMC5* cells transformed with the indicated centromeric plasmids. Glucose, *GAL* promoter off; galactose, *GAL* promoter on.
(E) Pull-down analysis of Smc5 sumoylation in *KR* mutants of the coiled-coil domain. S1, sumoylated species with lower electrophoretic mobility; S2, sumoylated species with higher electrophoretic mobility. Bottom panel: quantification of S1 and S2 Smc5-SUMO species from five independent pull-down experiments.
In (B), (C), and (E), circles indicate individual measurements, and red lines indicate mean values. p values were calculated using one-way ANOVA; only statistically significant p values are shown. See also Figure S2A.

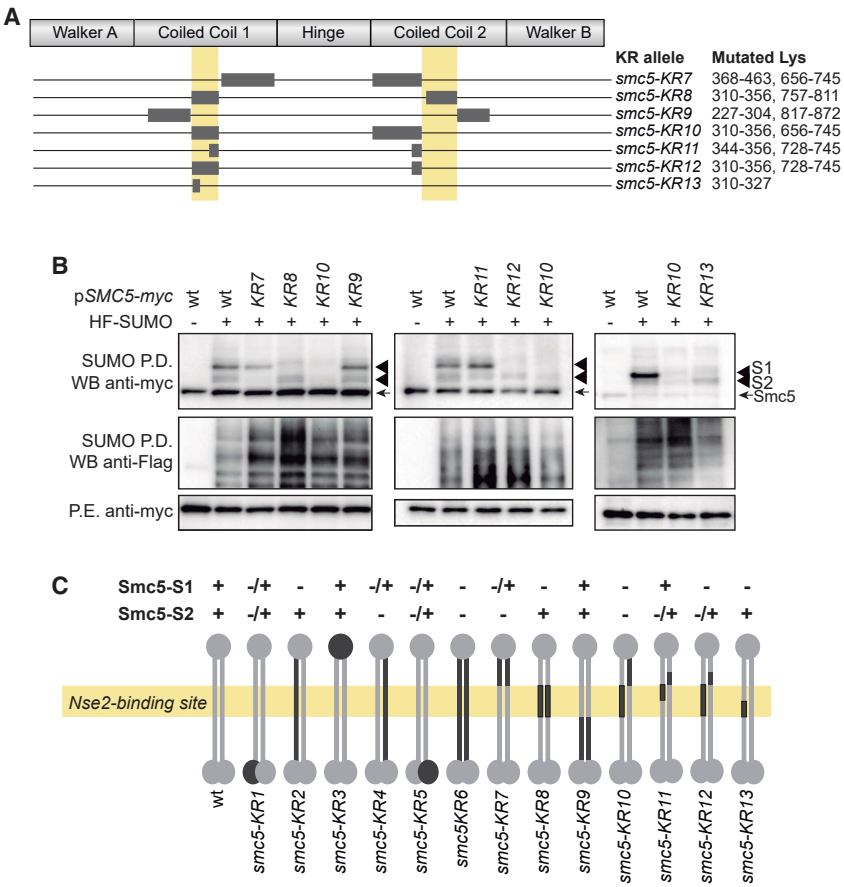

Figure 3. Identification of SUMO Acceptor Sites in the Coiled-Coil Domain of Smc5

(A) Summary of the *KR* alleles generated in this study, including affected domain/subdomain (in dark gray) and position of mutated lysines. Yellow boxes indicate the Nse2-binding region in Smc5.

(B) Exponentially growing cultures of the indicated strains were collected and analyzed using pull-down of HF-SUMO. Western blots in the left and middle panels are from cells expressing *SMC5* alleles from centromeric plasmids; western blot shown in the right panel is from cells expressing *SMC5* alleles from the endogenous *SMC5* locus. S1, sumoylated species with lower electrophoretic mobility; S2, sumoylated species with higher electrophoretic mobility. See also Figures S2B S3.

(C) Graphical depiction of the Smc5 mutant proteins generated in this study, indicating the position of the mutated lysine residues (in black) in the folded coiled coil structure of Smc5. The sumoylation state in Smc5 (Smc5-SUMO) is indicated as + (WT sumoylation), +/− or −/+ (partial sumoylation), and − (severely affected sumoylation).

See also Figure S3.

sumoylation may not have a net impact on DNA repair. To test if the *KR* mutations in the coiled coil affect the SUMO ligase in Nse2, we monitored sumoylation of Smc6 after Smc5 depletion in *smc5-aid* cells. Pull-down analysis indicated that Smc6 sumoylation levels were similar in cells ectopically expressing wild-type *SMC5* or the *smc5-KR10* mutant allele (Figure 4B). However, and in accordance with MMS sensitivity, we detected reduced levels of Smc6 sumoylation in *smc5-KR6* cells. This observation indicates that the Nse2 SUMO ligase is not fully functional in *smc5-KR6* cells. We speculate that the MMS sensitivity of *smc5-KR6* mutants is due to a structural alteration in the coiled-coil domain and the concomitant acquisition of a hypomorphic phenotype.

Mutations that prevent Smc5 sumoylation lie close to the Nse2 binding site. Therefore, the *smc5-KR10* allele could indirectly affect Smc5 sumoylation by altering the integrity of the Smc5/6 complex. We thus tested the Nse2-Smc5 interaction using co-immunoprecipitation analysis. As shown in Figure 4C, similar levels of the Nse2 subunit interacted with either wild-type or mutant proteins. The *smc5-KR10* mutation also did not seem to reduce the binding to the Nse4 kleisin subunit (Figure 4C). We have recently shown that the activity of the Nse2 SUMO ligase is modulated by binding of Smc5 to DNA. Decreased Smc5 sumoylation could therefore be due to defective loading of the Smc5/6 complex onto DNA. Chromosome spreads can be used to estimate changes in binding of Smc5/6 complexes to chromatin (Jeppsson et al., 2014; Varejão et al., 2018). As shown in Figure 4D, the *smc5-KR10* and *smc5-KR13* alleles did not significantly alter the association of Smc5 with chromatin. These results indicate that *smc5-KR10* prevents sumoylation of Smc5 without affecting the binding of the SUMO ligase to its docking site, its E3 activity, the integrity of the Smc5/6 complex, or binding of Smc5 to chromatin.

Smc5 Sumoylation Promotes SCJs in the rDNA Locus

Because Smc5 sumoylation is enhanced by replication fork damage, we reasoned that *smc5-KR10* mutant cells could display impairments in fork progression upon encounter with DNA lesions. Forks stalled at DNA lesions are frequently channeled into tolerance pathways to enable DNA synthesis and prevent fork collapse. The error-free branch of the DNA damage tolerance pathway promotes template switch behind the fork, leading to the formation of X-shaped sister chromatid junctions (SCJs). These structures can be detected using 2D gel electrophoresis in cells replicating in the presence of DNA damage. Under these conditions, mutations in the STR complex accumulate SCJs (Branzei et al., 2008; Fumasoni et al., 2015). SCJs in the rDNA locus were observed by 2D gel in single *sgs1Δ* mutant cells after release from a G1 cell-cycle arrest into 0.03% MMS, but not under unchallenged condition (Figures 5A and 5B). To our surprise, the *smc5-KR10* allele substantially reduced the amount of SCJs in *sgs1Δ* mutant cells. These results suggest that sumoylation of Smc5 promotes strand exchange during replication of a damaged DNA template.

Rad5-Mms2/Ubc13 triggers template switch through poly-ubiquitination of PCNA (Pol30 in budding yeast) (Branzei

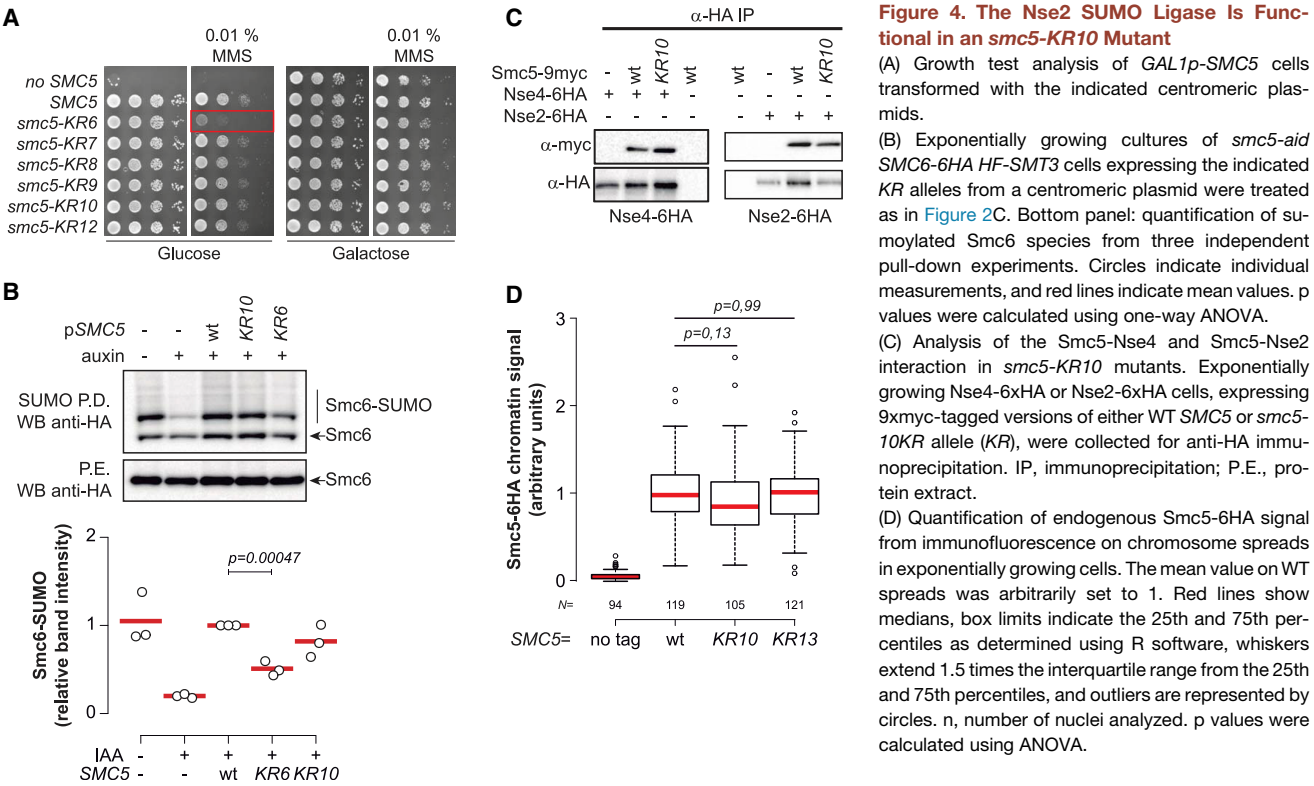

Figure 4. The Nse2 SUMO Ligase Is Functional in an *smc5-KR10* Mutant

(A) Growth test analysis of *GAL1p-SMC5* cells transformed with the indicated centromeric plasmids.

(B) Exponentially growing cultures of *smc5-aid SMC6-6HA HF-SMT3* cells expressing the indicated *KR* alleles from a centromeric plasmid were treated as in Figure 2C. Bottom panel: quantification of sumoylated Smc6 species from three independent pull-down experiments. Circles indicate individual measurements, and red lines indicate mean values. p values were calculated using one-way ANOVA.

(C) Analysis of the Smc5-Nse4 and Smc5-Nse2 interaction in *smc5-KR10* mutants. Exponentially growing Nse4-6xHA or Nse2-6xHA cells, expressing 9xmyc-tagged versions of either WT *SMC5* or *smc5-10KR* allele (*KR*), were collected for anti-HA immunoprecipitation. IP, immunoprecipitation; P.E., protein extract.

(D) Quantification of endogenous Smc5-6HA signal from immunofluorescence on chromosome spreads in exponentially growing cells. The mean value on WT spreads was arbitrarily set to 1. Red lines show medians, box limits indicate the 25th and 75th percentiles as determined using R software, whiskers extend 1.5 times the interquartile range from the 25th and 75th percentiles, and outliers are represented by circles. n, number of nuclei analyzed. p values were calculated using ANOVA.

et al., 2008). To analyze a possible role for Smc5 sumoylation in template switch, we analyzed the modification status of PCNA by western blot. Pol30 ubiquitylation (mono- and poly-ubiquitylation) was triggered in response to MMS-induced damage, and this effect was suppressed in *mms2Δ* and *pol30-K164R* mutants (Figure 5C). As sumoylated Pol30 (*SIZ1*-dependent) and di-ubiquitylated Pol30 (*MMS2*-dependent) forms ran very close to each other in western blots (Papouli et al., 2005; Hoege et al., 2002; Pfander et al., 2005), we used strains that carry a 6his-FLAG (HF) tag on SUMO to increase the molecular weight of the sumoylated Pol30 species. As shown in Figure 5C, Pol30 modifications were not substantially different in wild-type and *smc5-KR10* cells, suggesting that Smc5 sumoylation acts in a different pathway from, or downstream of, PCNA poly-ubiquitination.

Smc5 Sumoylation Is Functionally Linked to Mph1

DNA lesions that are not bypassed by strand exchange are frequently channeled into the error-prone translesion synthesis (TLS) pathway (Branzei and Psakhye, 2016; Schürer et al., 2004). TLS involves replication of the damaged template by the mutagenic Rev3 DNA polymerase, increasing the mutagenesis rate. *smc5-KR10* cells showed a 2.6-fold increase in the spontaneous mutagenesis rate (Figure 6A). This increase was dependent on *REV3*, which accounts for most mutagenic events in yeast (Figure 6A). These results indicate that defects in strand exchange at the fork are compensated by higher use of the Rev3 TLS polymerase in *smc5-KR10* cells.

Apart from PCNA-based DNA damage tolerance mechanisms, there are other means to bypass DNA lesions. Members of the FANCM family of motor proteins, including the budding yeast Mph1 ortholog, have fork regression activities capable of promoting template switch at the fork (Sun et al., 2008; Chen et al., 2009; Choi et al., 2010; Blackford et al., 2012). In addition, the lack of fork regression in *mph1Δ* cells leads to higher usage of Rev3-dependent translesion synthesis (Figure 6A) (Scheller et al., 2000). Interestingly, the *smc5-KR10* mutation did not increase mutagenesis levels in *mph1Δ* cells (Figure 6A). In accordance, *smc5-KR10* did not increase the MMS sensitivity of *mph1Δ* cells (Figure S4A). Moreover, *mph1Δ* and *smc5-KR10* were epistatic for MMS sensitivity in *mms4Δ* or *sgs1Δ* backgrounds (Figure 6B), mutations that sensitize *smc5-KR10* cells to MMS (see below). These observations indicate that Smc5 sumoylation and *MPH1* are epistatic for spontaneous mutagenesis and DNA damage sensitivity, suggesting that sumoylation of Smc5 is functionally connected to Mph1 at the molecular level.

Smc5 interacts with the Mph1 protein through the coiled-coil domain, and this interaction directly inhibits the fork regression activity of Mph1 (Xue et al., 2014). As the coiled-coil domain in Smc5 is also targeted by SUMO, we considered the possibility that Smc5 sumoylation could affect the interaction with Mph1. As shown in Figure 6C, Mph1 was able to co-immunoprecipitate equal amounts of either wild-type Smc5 or KR10 mutant proteins, indicating that Smc5 sumoylation does not affect its binding to Mph1. The histone fold MHF complex modulates Mph1 functions by relieving Smc5-dependent inhibition of

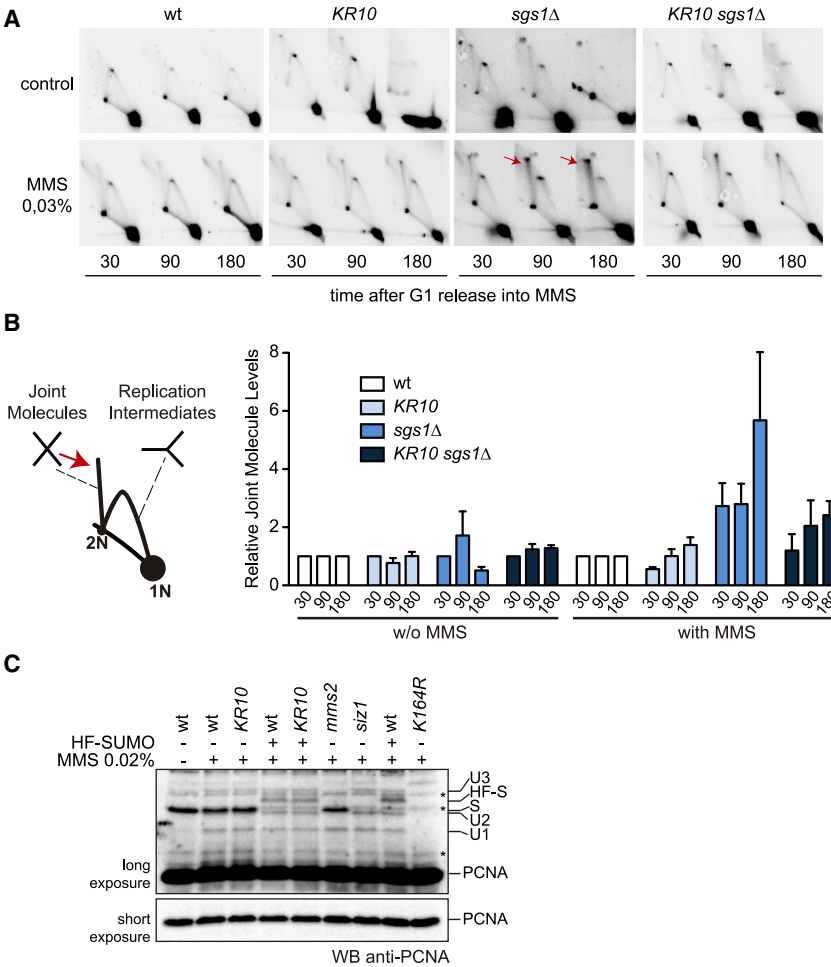

Figure 5. Accumulation of SCJs in *smc5-KR10* Unsumoylatable Mutant Cells

(A) Two-dimensional gel analysis of WT, *smc5-KR10*, *sgs1Δ*, and double *smc5-KR10 sgs1Δ* mutant cells. Cultures were released from a synchronous arrest in G1 into 0.03% MMS and samples taken at the indicated time after G1. Red arrows indicate joint molecules accumulating in MMS-treated *sgs1Δ* cells.

(B) Quantification of the joint molecules shown in (A). Bars indicate mean value and SEM of three independent experiments. Plotted values are normalized to the WT strain at each time point. Comparing *sgs1Δ* and *smc5-KR10 sgs1Δ* mutants, the p value calculated using the Wilcoxon signed-rank test for the MMS treated samples was <0.05.

(C) Western blot analysis with anti-PCNA (anti-Pol30) antibodies of TCA-protein extracts from the indicated strains. Samples were treated with 0.02% MMS for 1 h as indicated. S, SUMO-K164; HF-S, 6his-FLAG-SUMO-K164; U1, PCNA mono-ubiquitylated at K164; U2, PCNA di-ubiquitylated at K164; U3, PCNA triubiquitylated at K164; WT, wild-type; *KR10*, *smc5-KR10*; *mms2Δ* (unable to poly-ubiquitylate PCNA, lacking U2 and U3 species); *siz1Δ* (unable to sumoylate PCNA, lacking main sumoylation band); *K164R*, *Pol30-K164R* (unable to sumoylate or ubiquitylate PCNA at K164). Asterisks mark bands recognized by the anti-PCNA antibody but not related to modifications on K164.

Mph1 (Xue et al., 2015). Interestingly, we observed that Mhf1-TAP immunoprecipitated lower amounts of the Smc5-KR10 protein, suggesting that sumoylation of Smc5 may actually stimulate the Mhf1-Smc5 interaction (Figure 6D).

Mph1 can also disrupt D-loops during repair of double-stranded breaks [DSBs], thereby inhibiting break-induced replication (BIR) (Prakash et al., 2009; Luke-Glaser and Luke, 2012). Notably, this function is not regulated by Smc5 or the MHF complex (Xue et al., 2014, 2015). To measure if Smc5 sumoylation affects DSB repair, we tested BIR in a yeast strain that carries a truncated *ura3* allele next to an *HO* endonuclease site. Upon HO induction, the break is repaired using an homologous sequence on the other arm of the chromosome, restoring a functional *URA3* gene (Anand et al., 2014) (Figure S4B). Importantly, *mph1Δ* cells show a higher frequency of *URA3* cells after *HO* expression (Yimit et al., 2016). In contrast, the *smc5-KR10* mutation did not significantly alter the level of BIR (Figure S4C). Overall, our observations are in agreement with Smc5 sumoylation regulating only replication-associated repair (and not DSB repair) Mph1 roles, by helping relieve the negative regulation on Mph1 at damaged forks. This in turn would endorse fork regression and lower usage of translesion synthesis (Figure 6E).

A Deficiency in Smc5 Sumoylation Is Compensated by Structure-Specific Nucleases and Helicases

The lack of DNA-damage sensitivity of *smc5-KR10* is at odds with the observation that MMS induces Smc5 sumoylation (Figure 1). Consequently, we reasoned that Smc5 sumoylation might be normally redundant with pathways required to maintain the integrity of the genome. To study this possibility, we crossed *smc5-KR* cells with genes previously related to Smc5/6 function.

smc5-KR10 mutant cells showed a strong synthetic fitness defect in combination with *mms4* and *esc2* in the presence of MMS (Figure 7A; Figure S5A). Esc2 has been recently shown to directly stimulate the endonuclease activity of the Mms4-Mus81 complex (Sebesta et al., 2017). These interactions are also exhibited by the *smc5-KR13* allele, indicating that the synthetic sick defect is due mostly to reduced sumoylation in coiled coil 1 (Figure S5B). Additionally, we detected a mild synthetic sick phenotype of *smc5-KR10* in combination with mutations in the *SLX4* nuclease and the *RRM3* helicase (Figure S5C). Therefore, the deficiency in Smc5 sumoylation is normally compensated by the activity of structure selective nucleases and helicases. Even though Mus81-Mms4 and Slx4 are functionally connected through Cdk-dependent phosphorylation (Gritenaite et al., 2014), disruption of this interaction in *slx4-S486A* cells was not synthetic sick with *smc5-KR10* (Figure S5D).

Mms4-Mus81 operates late in the cell cycle to cleave sister chromatid junctions that prevent chromosome disjunction

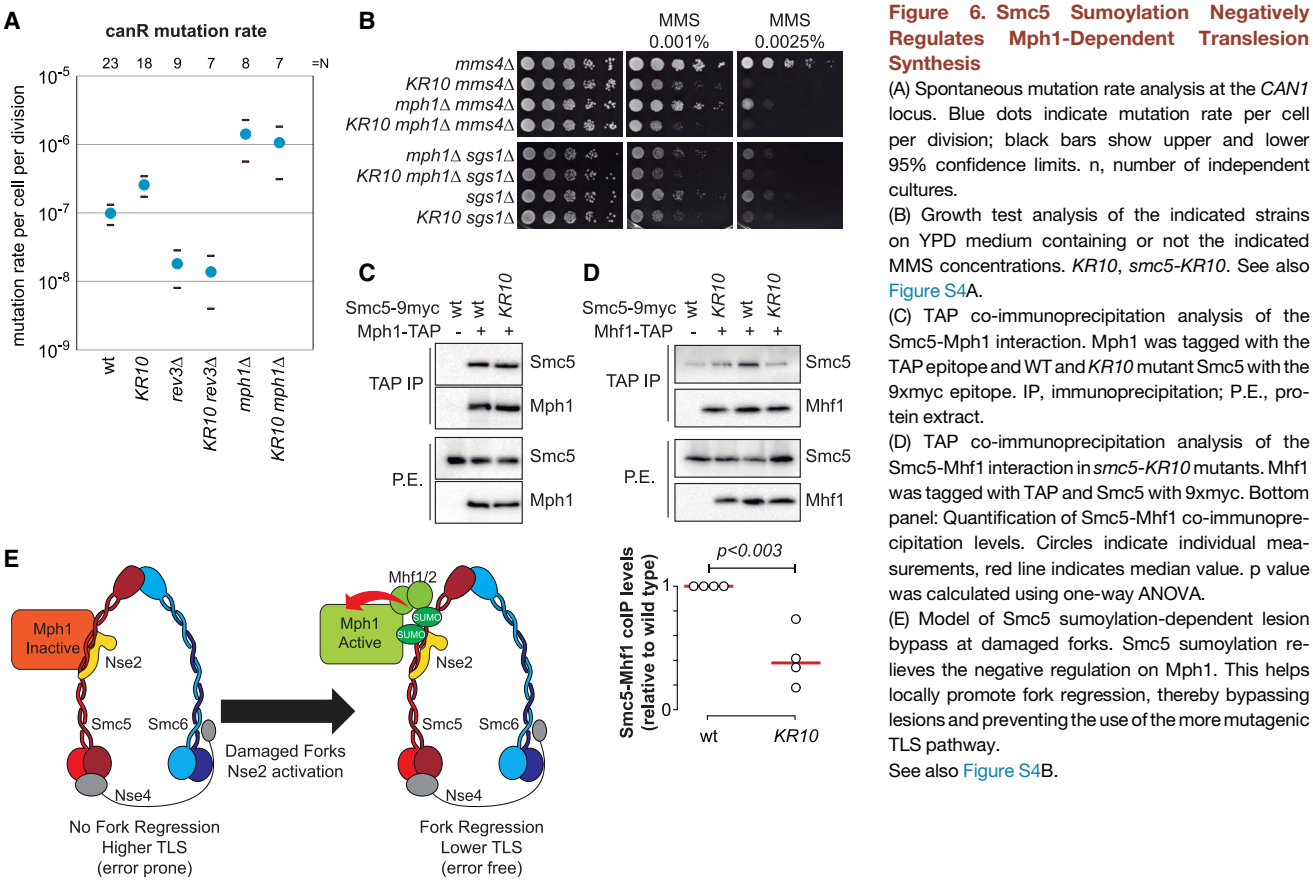

Figure 6. Smc5 Sumoylation Negatively Regulates Mph1-Dependent Translesion Synthesis

(A) Spontaneous mutation rate analysis at the *CAN1* locus. Blue dots indicate mutation rate per cell per division; black bars show upper and lower 95% confidence limits. n, number of independent cultures.

(B) Growth test analysis of the indicated strains on YPD medium containing or not the indicated MMS concentrations. *KR10*, *smc5-KR10*. See also Figure S4A.

(C) TAP co-immunoprecipitation analysis of the Smc5-Mph1 interaction. Mph1 was tagged with the TAP epitope and WT and *KR10* mutant Smc5 with the 9xmyc epitope. IP, immunoprecipitation; P.E., protein extract.

(D) TAP co-immunoprecipitation analysis of the Smc5-Mhf1 interaction in *smc5-KR10* mutants. Mhf1 was tagged with TAP and Smc5 with 9xmyc. Bottom panel: Quantification of Smc5-Mhf1 co-immunoprecipitation levels. Circles indicate individual measurements, red line indicates median value. p value was calculated using one-way ANOVA.

(E) Model of Smc5 sumoylation-dependent lesion bypass at damaged forks. Smc5 sumoylation relieves the negative regulation on Mph1. This helps locally promote fork regression, thereby bypassing lesions and preventing the use of the more mutagenic TLS pathway.

See also Figure S4B.

(Matos et al., 2011; Szakal and Branzei, 2013; Gallo-Fernández et al., 2012). The synthetic sickness of *smc5-KR10 mms4Δ* double mutants suggests that some replication forks not properly processed in *smc5-KR10* cells may later require cleavage by the nuclease. Inactivation of both mechanisms should therefore lead to accumulation of unprocessed forks at the time of chromosome segregation, potentially affecting chromosome disjunction. To test this possibility, we synchronized wild-type, *smc5-KR10*, *mms4Δ*, and double *smc5-KR10 mms4Δ* cells in G1. Cells were then treated with 0.01% MMS for 30 min to induce alkylation damage and were subsequently released into a synchronous cell cycle in the absence of MMS. Importantly, these conditions do not trigger a checkpoint response (Bermúdez-López et al., 2010). As shown in Figure 7B, all cells entered anaphase 60–75 min after release from G1. However, we noticed that double *smc5-KR10 mms4Δ* cells displayed larger numbers of anaphase figures, particularly at later time points (90 min onward); this phenotype was accompanied by lower number of cells with two segregated nuclei and higher levels of cells with unequal segregation of nuclear masses (nuclear missegregation; Figures 7B–7D). Therefore, we conclude that Mms4 and Smc5 sumoylation act in parallel pathways in response to alkylation damage to ensure chromosome segregation.

DISCUSSION

Here we have shown that Smc5 is preferentially sumoylated under conditions of replication fork damage, in a pattern that is remarkably different from other Nse2-dependent substrates. Our analysis indicates that Smc5 sumoylation is a specific read-out for replication fork damage, responding differently to paused or damaged replication forks and to replication-dependent or replication-independent double-stranded breaks. From a more mechanistic point of view, our findings are consistent with lower activity of the Mph1 motor protein, a fork regression enzyme that normally contributes to lesion bypass at the fork (Xue et al., 2014, 2015), in *smc5-KR* mutant cells (Figure 6E). In accordance, deficient sumoylation of Smc5 leads to reduced formation of sister chromatid junctions in the rDNA and favors the use of the more mutagenic translesion synthesis pathway. Altogether, our results point toward the participation of Smc5 sumoylated species in DDT.

A Potential Mechanism for Smc5 Sumoylation in Lesion Bypass

Smc5 is part of the Smc5/6 complex, and several of its subunits are also targeted by SUMO (Bermúdez-López et al., 2016). SUMO often targets protein complexes or groups of physically connected proteins, what has been referred to as protein

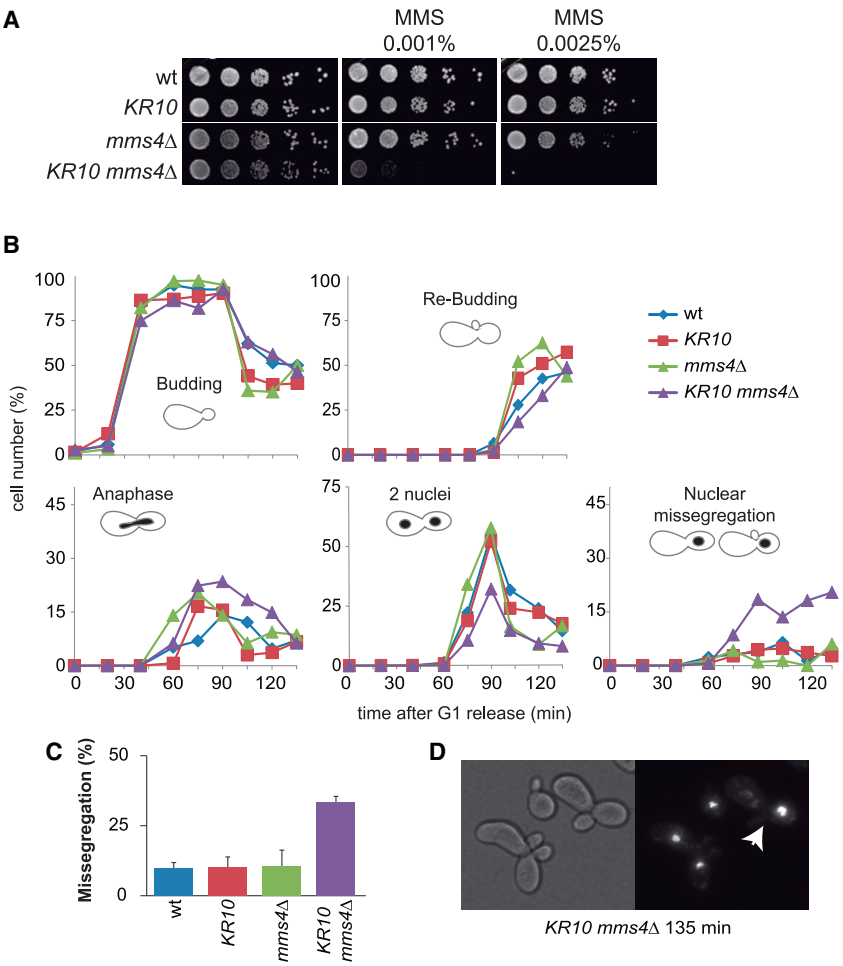

Figure 7. The *smc5-KR10* Mutant Is Compensated by Structure-Specific Nucleases and Helicases

(A) Growth test analysis of WT, *smc5-KR10* (*KR10*), *mms4Δ*, and double *mms4Δ smc5-KR10* cells; 10-fold serial dilutions of the liquid cultures were spotted in YPD in the presence of the indicated MMS concentrations and pictures taken after 48 h. See also Figures S5 and S6.

(B) Cells of the indicated genotype were synchronized in G1 with alpha factor, treated with MMS 0.01% for 30 min, and released into a synchronous cell cycle in the absence of MMS. Samples were taken at the indicated time points for microscopic analysis and scored for budding (first S phase), re-budding (second S phase), elongated nucleus between mother and daughter cell (anaphase), two nuclei (two nuclear masses between mother cell and bud), and nuclear missegregation (unequal segregation of nuclear masses).

(C) Quantification of nuclear missegregation from three independent experiments. Bars indicate means, error bars are SEM.

(D) Example of double-mutant cells at a late time point. Arrow points to a cell with nuclear segregation defects.

group sumoylation (Psakhye and Jentsch, 2012). Protein group sumoylation functions as a molecular glue. Importantly, our results demonstrate that sumoylation of an individual component in a protein complex can have its own role, beyond its putative synergistic effect with other sumoylated subunits. Although we have not examined the role of sumoylation in other Smc5/6 subunits, we cannot exclude that they also participate in, or even reinforce, bypass of fork damage. Our results suggest that sumoylation of Smc5 might create a molecular environment that relieves the negative regulation on Mph1-dependent fork regression, maybe by increasing the frequency of Smc5-Mhf1 interactions. The epistatic effect of *smc5-KR10* mutants on the MMS sensitivity and mutation rate of *mph1Δ* cells also supports this model. It is worth noting that spontaneous mutagenesis in *mph1Δ* mutant cells is higher than in *smc5-KR10* cells. This observation reflects a firmer role for Mph1 than Smc5 sumoylation in suppressing TLS, suggesting that sumoylation of Smc5 only contributes to a subset of all Mph1-dependent fork bypass events.

It is currently unclear how MHF relieves Mph1 from Smc5 inhibition. Mph1 directly interacts with Smc5 and Mhf1, probably bridging an Smc5-Mph1-MHF trimeric interaction (Xue et al., 2016). It is therefore probable that MHF reactivates the fork regression activity of Mph1 without necessarily disengaging Smc5 from Mph1. Therefore, we envisage that Smc5 may be sumoylated in a small subset of damaged forks, enhancing Mph1-dependent fork regression. Mph1 would remain inhibited by Smc5 at most other damaged sites, requiring other means of DDT for lesion bypass. Previous works have shown that Mph1-dependent fork regression only justifies around one third of the SCJs accumulating in a specific region of chromosome 3 of *sgs1Δ* mutants (Mankouri et al., 2009; Chen et al., 2009). In contrast, our data suggest that Smc5 sumoylation could account for a larger fraction of the X-shaped molecules accumulating in the rDNA array (Figure 5). It is possible that Smc5 sumoylation and Mph1 play a more active role in regulating fork stability in the rDNA than in the rest of the genome. In accordance, the Smc5/6 complex is enriched in this locus, where it plays various roles to maintain its integrity (De Piccoli et al., 2009; Torres-Rosell et al., 2005). In addition, forks arrested by Fob1 at the replication fork barrier present in each repeat may promote replication fork regression (Peng et al., 2018). This could make this repetitive locus particularly susceptible to regulation by Smc5/6 and Mph1.

Smc5 Sumoylation Is Redundant with Other Pathways Operating at Damaged Replication Forks

Our genetic analysis indicates that the Mms4/Mus81 complex, as well as other nucleases/helicases, normally compensate defects in Smc5 sumoylation. Mms4/Mus81 has also been proposed to back up the STR complex in removal of template switch structures that persist in G2/M (Matos et al., 2011; Gallo-Fernández et al., 2012). However, Mms4/Mus81 plays a limited role in

resolution of template switch structures, and differently from *sgs1Δ* cells, *mms4Δ* mutant cells do not accumulate SCJs (Ashton et al., 2011). In contrast, activation of Mms4/Mus81 in G2/M is essential for completion of genome replication in the presence of DNA damage (Saugar et al., 2013), which suggests that Mms4/Mus81 may cleave replication forks blocked by DNA lesions in G2/M. In mammals, entry into mitosis also triggers recruitment of Eme1/Mus81 to forks stalled at chromosome fragile sites. Its nuclease activity then allows resumption of DNA synthesis, promoting chromosome disjunction (Minocherhomji et al., 2015). Therefore, Mms4/Mus81 helps complete genome replication by means different from resolution of template switch structures. In accordance, whereas *sgs1Δ* and *mms2Δ* are epistatic, *mms4Δ* and *mms2Δ* are additive for MMS sensitivity (Figure S6). We propose that forks that are left unprocessed in *smc5-KR* cells may require the action of different helicases/nucleases, including the Mms4/Mus81 complex, to reactivate them.

Although fork regression is generally accepted to occur in fission yeast and mammalian cells, these structures have not been detected using electron microscopy in wild-type budding yeast cells (Giannattasio et al., 2014). This suggests that they never form or are too short lived. It is also possible that regressed replication fork structures rapidly promote recombination by invading unreplicated parental strands ahead of the fork, creating SCJs. Several enzymatic activities, including helicases and nucleases, control the metabolism of regressed forks. Rad5 and Mph1, two helicases participating in lesion bypass, have been shown to mediate fork regression *in vitro* (Meng and Zhao, 2017). In addition, the Rrm3 and Pif1 helicases can also mediate fork regression *in vivo*, although this activity is normally restrained by the DNA damage checkpoint (Rossi et al., 2015). Therefore, the increased MMS sensitivity of double *rrm3Δ smc5-KR* mutant cells, relative to single mutants, might stem from a synergistic defect in promoting regression at damaged forks.

Smc5 Sumoylation Modulates an Early Recombinational Function of the Smc5/6 Complex

Smc5/6 plays an active role in removal of recombination-dependent junctions (Bermúdez-López et al., 2010; Chavez et al., 2010). Surprisingly, whereas SUMO ligase *nse2-CH* or *nse2ΔC* mutants lead to the accumulation of sister chromatid junctions (Branzei et al., 2006), *smc5-KR* unsumoylatable mutants actually reduced X-shaped intermediates. This difference may be due to the concurrent reduction in sumoylation of multiple SUMO targets in *nse2* mutants, including deficient activation of the STR complex (Bermúdez-López et al., 2016; Bonner et al., 2016). Our findings also suggest that sumoylation of Smc5 has roles distinct from resolution/dissolution of recombination intermediates, most probably at an early step during generation of joint molecules. Fission yeast and human cells may also trigger fork regression to protect replication forks. In fact, a similar "early role" has already been proposed in *S. pombe*, where Smc5/6 would promote RPA and Rad52 loading to stalled replication forks to keep them primed for restart (Irmisch et al., 2009). As Smc5/6 seems to have an early function in both yeasts, it will be interesting to test if the Smc5/SUMO-dependent mechanism described here is conserved in evolution, and participates as a safeguard fork protection mechanism in human cells.

STAR★METHODS

Detailed methods are provided in the online version of this paper and include the following:

- KEY RESOURCES TABLE
- LEAD CONTACT AND MATERIALS AVAILABILITY
- EXPERIMENTAL MODEL AND SUBJECT DETAILS
- METHOD DETAILS
  - Construction of mutants strains and plasmids
  - MMS sensitivity assays
  - Cell cycle experiments
  - Pull down analysis of sumoylated proteins
  - Co-immunoprecipitation analysis
  - Western blot analysis of PCNA modification
  - Mass spectrometry for identification of Smc5 sumoylation sites
  - 2D gel analysis of replication intermediates
  - Determination of spontaneous mutation rate and BIR assay
  - Chromosome spreads
- QUANTIFICATION AND STATISTICAL ANALYSIS
- DATA CODE AND AVAILABILITY

SUPPLEMENTAL INFORMATION

Supplemental Information can be found online at https://doi.org/10.1016/j.celrep.2019.10.123.

ACKNOWLEDGMENTS

Work in the J.T.-R. lab was supported by grants BFU2015-71308-P and PGC2018-097796-B-I00 from Ministerio de Ciencia, Innovación y Universidades and grant 2017-SGR-569 from AGAUR-Generalitat de Catalunya; the IRBLLEIDA Institute is part of CERCA Programme/Generalitat de Catalunya. R.W. was funded by grant BFU2015-69183-P. Work in the L.A. laboratory was supported by a Wellcome Trust Senior Investigator Award to L.A. (100955, "Functional Dissection of Mitotic Chromatin") and the London Institute of Medical Research (LMS), which receives its core funding from the UK Medical Research Council. We thank Laia de Nadal for the BY5563 yeast strain, Jim Haber for the BIR strain, Boris Pfander for the *slx4-S486A* mutant, and Patrick Sung for kindly sharing materials and helpful advice; Sònia Rius, Seba Almedawar, and Clàudia Guasch for construction of yeast strains and *smc5-KR* plasmids; Hélène Gaillard for analysis and statistical analysis of 2D gel intermediates; Carolina de la Torre for the proteomic analysis of Smc5-SUMO peptides; and Andrés Clemente, Jose Antonio Tercero, and all members of the Cell Cycle lab for helpful discussions.

AUTHOR CONTRIBUTIONS

I.P.-M., M.B.-L., N.C., and J.T.-R. designed and constructed *smc5-KR* mutants. M.Z., I.P.-M., M.B.-L., E.I., R.S.-S., S.A., N.C., and J.T.-R. conducted experiments. M.T. performed chromosome spreads. C.C. performed PCNA western blots. I.P.-M., H.H.-G., and R.W. conducted 2D gel experiments. P.G.-E. and L.A. conducted SUMO proteomics. R.W., N.C., and J.T.-R. analyzed results. J.T.-R. conceived the idea for the project and wrote the paper.

DECLARATION OF INTERESTS

The authors declare no competing interests.

Received: April 9, 2019
Revised: September 25, 2019
Accepted: October 29, 2019
Published: December 3, 2019

REFERENCES

Albuquerque, C.P., Wang, G., Lee, N.S., Kolodner, R.D., Putnam, C.D., and Zhou, H. (2013). Distinct SUMO ligases cooperate with Esc2 and Slx5 to suppress duplication-mediated genome rearrangements. PLoS Genet. *9*, e1003670.

Almedawar, S., Colomina, N., Bermudez-Lopez, M., Pociño-Merino, I., and Torres-Rosell, J. (2012). A SUMO-dependent step during establishment of sister chromatid cohesion. Curr. Biol. *22*, 1576–1581.

Anand, R.P., Tsaponina, O., Greenwell, P.W., Lee, C.-S., Du, W., Petes, T.D., and Haber, J.E. (2014). Chromosome rearrangements via template switching between diverged repeated sequences. Genes Dev. *28*, 2394–2406.

Andrews, E.A., Palecek, J., Sergeant, J., Taylor, E., Lehmann, A.R., and Watts, F.Z. (2005). Nse2, a component of the Smc5-6 complex, is a SUMO ligase required for the response to DNA damage. Mol. Cell. Biol. *25*, 185–196.

Ashton, T.M., Mankouri, H.W., Heidenblut, A., McHugh, P.J., and Hickson, I.D. (2011). Pathways for Holliday junction processing during homologous recombination in Saccharomyces cerevisiae. Mol. Cell. Biol. *31*, 1921–1933.

Bermúdez-López, M., Ceschia, A., de Piccoli, G., Colomina, N., Pasero, P., Aragón, L., and Torres-Rosell, J. (2010). The Smc5/6 complex is required for dissolution of DNA-mediated sister chromatid linkages. Nucleic Acids Res. *38*, 6502–6512.

Bermúdez-López, M., Pociño-Merino, I., Sánchez, H., Bueno, A., Guasch, C., Almedawar, S., Bru-Virgili, S., Garí, E., Wyman, C., Reverter, D., et al. (2015). ATPase-dependent control of the Mms21 SUMO ligase during DNA repair. PLoS Biol. *13*, e1002089.

Bermúdez-López, M., Villoria, M.T.M.T., Esteras, M., Jarmuz, A., Torres-Rosell, J., Clemente-Blanco, A., and Aragon, L. (2016). Sgs1's roles in DNA end resection, HJ dissolution, and crossover suppression require a two-step SUMO regulation dependent on Smc5/6. Genes Dev. *30*, 1339–1356.

Blackford, A.N., Schwab, R.A., Nieminuszczy, J., Deans, A.J., West, S.C., and Niedzwiedz, W. (2012). The DNA translocase activity of FANCM protects stalled replication forks. Hum. Mol. Genet. *21*, 2005–2016.

Bonner, J.N., Choi, K., Xue, X., Torres, N.P., Szakal, B., Wei, L., Wan, B., Arter, M., Matos, J., Sung, P., et al. (2016). Smc5/6 mediated sumoylation of the Sgs1-Top3-Rmi1 complex promotes removal of recombination intermediates. Cell Rep. *16*, 368–378.

Branzei, D., and Psakhye, I. (2016). DNA damage tolerance. Curr. Opin. Cell Biol. *40*, 137–144.

Branzei, D., and Szakal, B. (2017). Building up and breaking down: mechanisms controlling recombination during replication. Crit. Rev. Biochem. Mol. Biol. *52*, 381–394.

Branzei, D., Sollier, J., Liberi, G., Zhao, X., Maeda, D., Seki, M., Enomoto, T., Ohta, K., and Foiani, M. (2006). Ubc9- and mms21-mediated sumoylation counteracts recombinogenic events at damaged replication forks. Cell *127*, 509–522.

Branzei, D., Vanoli, F., and Foiani, M. (2008). SUMOylation regulates Rad18-mediated template switch. Nature *456*, 915–920.

Chavez, A., George, V., Agrawal, V., and Johnson, F.B. (2010). Sumoylation and the structural maintenance of chromosomes (Smc) 5/6 complex slow senescence through recombination intermediate resolution. J. Biol. Chem. *285*, 11922–11930.

Chavez, A., Agrawal, V., and Johnson, F.B. (2011). Homologous recombination-dependent rescue of deficiency in the structural maintenance of chromosomes (Smc) 5/6 complex. J. Biol. Chem. *286*, 5119–5125.

Chen, Y.H., Choi, K., Szakal, B., Arenz, J., Duan, X., Ye, H., Branzei, D., and Zhao, X. (2009). Interplay between the Smc5/6 complex and the Mph1 helicase in recombinational repair. Proc. Natl. Acad. Sci. U S A *106*, 21252–21257.

Choi, K., Szakal, B., Chen, Y.H., Branzei, D., and Zhao, X. (2010). The Smc5/6 complex and Esc2 influence multiple replication-associated recombination processes in Saccharomyces cerevisiae. Mol. Biol. Cell *21*, 2306–2314.

Cremona, C.A., Sarangi, P., Yang, Y., Hang, L.E., Rahman, S., and Zhao, X. (2012). Extensive DNA damage-induced sumoylation contributes to replication and repair and acts in addition to the mec1 checkpoint. Mol. Cell *45*, 422–432.

Daigaku, Y., Davies, A.A., and Ulrich, H.D. (2010). Ubiquitin-dependent DNA damage bypass is separable from genome replication. Nature *465*, 951–955.

de Bettignies, G., and Johnston, L.H. (2003). The mitotic exit network. Curr. Biol. *13*, R301.

De Piccoli, G., Torres-Rosell, J., and Aragón, L. (2009). The unnamed complex: what do we know about Smc5-Smc6? Chromosome Res. *17*, 251–263.

Duan, X., Yang, Y., Chen, Y.H., Arenz, J., Rangi, G.K., Zhao, X., and Ye, H. (2009). Architecture of the Smc5/6 complex of Saccharomyces cerevisiae reveals a unique interaction between the Nse5-6 subcomplex and the hinge regions of Smc5 and Smc6. J. Biol. Chem. *284*, 8507–8515.

Fumasoni, M., Zwicky, K., Vanoli, F., Lopes, M., and Branzei, D. (2015). Error-free DNA damage tolerance and sister chromatid proximity during DNA replication rely on the Polα/Primase/Ctf4 Complex. Mol. Cell *57*, 812–823.

Gallo-Fernández, M., Saugar, I., Ortiz-Bazán, M.Á., Vázquez, M.V., and Tercero, J.A. (2012). Cell cycle-dependent regulation of the nuclease activity of Mus81-Eme1/Mms4. Nucleic Acids Res. *40*, 8325–8335.

García-Rodríguez, N., Wong, R.P., and Ulrich, H.D. (2016). Functions of ubiquitin and SUMO in DNA replication and replication stress. Front. Genet. *7*, 87.

Giannattasio, M., Zwicky, K., Follonier, C., Foiani, M., Lopes, M., and Branzei, D. (2014). Visualization of recombination-mediated damage bypass by template switching. Nat. Struct. Mol. Biol. *21*, 884–892.

Gillet-Markowska, A., Louvel, G., and Fischer, G. (2015). bz-rates: a web tool to estimate mutation rates from fluctuation analysis. G3 (Bethesda) *5*, 2323–2327.

Goldstein, A.L., and McCusker, J.H. (1999). Three new dominant drug resistance cassettes for gene disruption in Saccharomyces cerevisiae. Yeast *15*, 1541–1553.

Gritenaite, D., Princz, L.N., Szakal, B., Bantele, S.C.S., Wendeler, L., Schilbach, S., Habermann, B.H., Matos, J., Lisby, M., Branzei, D., and Pfander, B. (2014). A cell cycle-regulated Slx4-Dpb11 complex promotes the resolution of DNA repair intermediates linked to stalled replication. Genes Dev. *28*, 1604–1619.

Grubb, J., Brown, M.S., and Bishop, D.K. (2015). Surface spreading and immunostaining of yeast chromosomes. J. Vis. Exp. (*102*), e53081.

Hoege, C., Pfander, B., Moldovan, G.L., Pyrowolakis, G., and Jentsch, S. (2002). RAD6-dependent DNA repair is linked to modification of PCNA by ubiquitin and SUMO. Nature *419*, 135–141.

Irmisch, A., Ampatzidou, E., Mizuno, K., O'Connell, M.J., and Murray, J.M. (2009). Smc5/6 maintains stalled replication forks in a recombination-competent conformation. EMBO J. *28*, 144–155.

Janke, C., Magiera, M.M., Rathfelder, N., Taxis, C., Reber, S., Maekawa, H., Moreno-Borchart, A., Doenges, G., Schwob, E., Schiebel, E., and Knop, M. (2004). A versatile toolbox for PCR-based tagging of yeast genes: new fluorescent proteins, more markers and promoter substitution cassettes. Yeast *21*, 947–962.

Jeppsson, K., Carlborg, K.K., Nakato, R., Berta, D.G., Lilienthal, I., Kanno, T., Lindqvist, A., Brink, M.C., Dantuma, N.P., Katou, Y., et al. (2014). The chromosomal association of the Smc5/6 complex depends on cohesion and predicts the level of sister chromatid entanglement. PLoS Genet. *10*, e1004680.

Karras, G.I., and Jentsch, S. (2010). The RAD6 DNA damage tolerance pathway operates uncoupled from the replication fork and is functional beyond S phase. Cell *141*, 255–267.

Kegel, A., and Sjögren, C. (2010). The Smc5/6 complex: more than repair? Cold Spring Harb. Symp. Quant. Biol. *75*, 179–187.

Lambert, S., and Carr, A.M. (2013). Replication stress and genome rearrangements: lessons from yeast models. Curr. Opin. Genet. Dev. *23*, 132–139.

Lehmann, A.R., Niimi, A., Ogi, T., Brown, S., Sabbioneda, S., Wing, J.F., Kannouche, P.L., and Green, C.M. (2007). Translesion synthesis: Y-family polymerases and the polymerase switch. DNA Repair (Amst.) *6*, 891–899.

Lopes, M., Cotta-Ramusino, C., Pellicioli, A., Liberi, G., Plevani, P., Muzi-Falconi, M., Newlon, C.S., and Foiani, M. (2001). The DNA replication checkpoint response stabilizes stalled replication forks. Nature *412*, 557–561.

Luke-Glaser, S., and Luke, B. (2012). The Mph1 helicase can promote telomere uncapping and premature senescence in budding yeast. PLoS ONE *7*, e42028.

Mankouri, H.W., Ngo, H.P., and Hickson, I.D. (2009). Esc2 and Sgs1 act in functionally distinct branches of the homologous recombination repair pathway in Saccharomyces cerevisiae. Mol. Biol. Cell *20*, 1683–1694.

Matos, J., and West, S.C. (2014). Holliday junction resolution: regulation in space and time. DNA Repair (Amst.) *19*, 176–181.

Matos, J., Blanco, M.G., Maslen, S., Skehel, J.M., and West, S.C. (2011). Regulatory control of the resolution of DNA recombination intermediates during meiosis and mitosis. Cell *147*, 158–172.

McAleenan, A., Cordon-Preciado, V., Clemente-Blanco, A., Liu, I.C., Sen, N., Leonard, J., Jarmuz, A., and Aragón, L. (2012). SUMOylation of the α-kleisin subunit of cohesin is required for DNA damage-induced cohesion. Curr. Biol. *22*, 1564–1575.

Meng, X., and Zhao, X. (2017). Replication fork regression and its regulation. FEMS Yeast Res. *17*, fow110.

Menolfi, D., Delamarre, A., Lengronne, A., Pasero, P., and Branzei, D. (2015). Essential roles of the Smc5/6 complex in replication through natural pausing sites and endogenous DNA damage tolerance. Mol. Cell *60*, 835–846.

Minocherhomji, S., Ying, S., Bjerregaard, V.A., Bursomanno, S., Aleliunaite, A., Wu, W., Mankouri, H.W., Shen, H., Liu, Y., and Hickson, I.D. (2015). Replication stress activates DNA repair synthesis in mitosis. Nature *528*, 286–290.

Mizuno, K., Miyabe, I., Schalbetter, S.A., Carr, A.M., and Murray, J.M. (2013). Recombination-restarted replication makes inverted chromosome fusions at inverted repeats. Nature *493*, 246–249.

Nishimura, K., Fukagawa, T., Takisawa, H., Kakimoto, T., and Kanemaki, M. (2009). An auxin-based degron system for the rapid depletion of proteins in nonplant cells. Nat. Methods *6*, 917–922.

Papouli, E., Chen, S., Davies, A.A., Huttner, D., Krejci, L., Sung, P., and Ulrich, H.D. (2005). Crosstalk between SUMO and ubiquitin on PCNA is mediated by recruitment of the helicase Srs2p. Mol. Cell *19*, 123–133.

Peng, X.P., Lim, S., Li, S., Marjavaara, L., Chabes, A., and Zhao, X. (2018). Acute Smc5/6 depletion reveals its primary role in rDNA replication by restraining recombination at fork pausing sites. PLoS Genet. *14*, e1007129.

Pfander, B., Moldovan, G.L., Sacher, M., Hoege, C., and Jentsch, S. (2005). SUMO-modified PCNA recruits Srs2 to prevent recombination during S phase. Nature *436*, 428–433.

Pond, K.W., de Renty, C., Yagle, M.K., and Ellis, N.A. (2019). Rescue of collapsed replication forks is dependent on NSMCE2 to prevent mitotic DNA damage. PLoS Genet. *15*, e1007942.

Potts, P.R., and Yu, H. (2005). Human MMS21/NSE2 is a SUMO ligase required for DNA repair. Mol. Cell Biol. *25*, 7021–7032.

Prakash, R., Satory, D., Dray, E., Papusha, A., Scheller, J., Kramer, W., Krejci, L., Klein, H., Haber, J.E., Sung, P., and Ira, G. (2009). Yeast Mph1 helicase dissociates Rad51-made D-loops: implications for crossover control in mitotic recombination. Genes Dev. *23*, 67–79.

Psakhye, I., and Jentsch, S. (2012). Protein group modification and synergy in the SUMO pathway as exemplified in DNA repair. Cell *151*, 807–820.

Rossi, S.E., Ajazi, A., Carotenuto, W., Foiani, M., and Giannattasio, M. (2015). Rad53-mediated regulation of Rrm3 and Pif1 DNA helicases contributes to prevention of aberrant fork transitions under replication stress. Cell Rep. *13*, 80–92.

Saugar, I., Vázquez, M.V., Gallo-Fernández, M., Ortiz-Bazán, M.Á., Segurado, M., Calzada, A., and Tercero, J.A. (2013). Temporal regulation of the Mus81-Mms4 endonuclease ensures cell survival under conditions of DNA damage. Nucleic Acids Res. *41*, 8943–8958.

Scheller, J., Schürer, A., Rudolph, C., Hettwer, S., and Kramer, W. (2000). MPH1, a yeast gene encoding a DEAH protein, plays a role in protection of the genome from spontaneous and chemically induced damage. Genetics *155*, 1069–1081.

Schürer, K.A., Rudolph, C., Ulrich, H.D., and Kramer, W. (2004). Yeast MPH1 gene functions in an error-free DNA damage bypass pathway that requires genes from Homologous recombination, but not from postreplicative repair. Genetics *166*, 1673–1686.

Sebesta, M., Urulangodi, M., Stefanovie, B., Szakal, B., Pacesa, M., Lisby, M., Branzei, D., and Krejci, L. (2017). Esc2 promotes Mus81 complex-activity via its SUMO-like and DNA binding domains. Nucleic Acids Res. *45*, 215–230.

Sogo, J.M., Lopes, M., and Foiani, M. (2002). Fork reversal and ssDNA accumulation at stalled replication forks owing to checkpoint defects. Science *297*, 599–602.

Sun, W., Nandi, S., Osman, F., Ahn, J.S., Jakovleska, J., Lorenz, A., and Whitby, M.C. (2008). The FANCM ortholog Fml1 promotes recombination at stalled replication forks and limits crossing over during DNA double-strand break repair. Mol. Cell *32*, 118–128.

Szakal, B., and Branzei, D. (2013). Premature Cdk1/Cdc5/Mus81 pathway activation induces aberrant replication and deleterious crossover. EMBO J. *32*, 1155–1167.

Tercero, J.A., and Diffley, J.F. (2001). Regulation of DNA replication fork progression through damaged DNA by the Mec1/Rad53 checkpoint. Nature *412*, 553–557.

Torres-Rosell, J., Machín, F., Farmer, S., Jarmuz, A., Eydmann, T., Dalgaard, J.Z., and Aragón, L. (2005). SMC5 and SMC6 genes are required for the segregation of repetitive chromosome regions. Nat. Cell Biol. *7*, 412–419.

Torres-Rosell, J., De Piccoli, G., Cordon-Preciado, V., Farmer, S., Jarmuz, A., Machin, F., Pasero, P., Lisby, M., Haber, J.E., and Aragón, L. (2007). Anaphase onset before complete DNA replication with intact checkpoint responses. Science *315*, 1411–1415.

Urulangodi, M., Sebesta, M., Menolfi, D., Szakal, B., Sollier, J., Sisakova, A., Krejci, L., and Branzei, D. (2015). Local regulation of the Srs2 helicase by the SUMO-like domain protein Esc2 promotes recombination at sites of stalled replication. Genes Dev. *29*, 2067–2080.

Varejão, N., Ibars, E., Lascorz, J., Colomina, N., Torres-Rosell, J., and Reverter, D. (2018). DNA activates the Nse2/Mms21 SUMO E3 ligase in the Smc5/6 complex. EMBO J. *37*, e98306.

Wellinger, R.E., Schär, P., and Sogo, J.M. (2003). Rad52-independent accumulation of joint circular minichromosomes during S phase in Saccharomyces cerevisiae. Mol. Cell. Biol. *23*, 6363–6372.

Whitby, M.C. (2010). The FANCM family of DNA helicases/translocases. DNA Repair (Amst.) *9*, 224–236.

Xue, X., Choi, K., Bonner, J., Chiba, T., Kwon, Y., Xu, Y., Sanchez, H., Wyman, C., Niu, H., Zhao, X., and Sung, P. (2014). Restriction of replication fork regression activities by a conserved SMC complex. Mol. Cell *56*, 436–445.

Xue, X., Choi, K., Bonner, J.N., Szakal, B., Chen, Y.H., Papusha, A., Saro, D., Niu, H., Ira, G., Branzei, D., et al. (2015). Selective modulation of the functions of a conserved DNA motor by a histone fold complex. Genes Dev. *29*, 1000–1005.

Xue, X., Papusha, A., Choi, K., Bonner, J.N., Kumar, S., Niu, H., Kaur, H., Zheng, X.F., Donnianni, R.A., Lu, L., et al. (2016). Differential regulation of the anti-crossover and replication fork regression activities of Mph1 by Mte1. Genes Dev. *30*, 687–699.

Yimit, A., Kim, T., Anand, R.P., Meister, S., Ou, J., Haber, J.E., Zhang, Z., and Brown, G.W. (2016). MTE1 functions with MPH1 in double-strand break repair. Genetics *203*, 147–157.

Zhang, H., and Lawrence, C.W. (2005). The error-free component of the RAD6/RAD18 DNA damage tolerance pathway of budding yeast employs sister-strand recombination. Proc. Natl. Acad. Sci. U S A *102*, 15954–15959.

Zhao, X., and Blobel, G. (2005). A SUMO ligase is part of a nuclear multiprotein complex that affects DNA repair and chromosomal organization. Proc. Natl. Acad. Sci. U S A *102*, 4777–4782.

Zou, L., and Elledge, S.J. (2003). Sensing DNA damage through ATRIP recognition of RPA-ssDNA complexes. Science *300*, 1542–1548.

STAR★METHODS

KEY RESOURCES TABLE

REAGENT or RESOURCE	SOURCE	IDENTIFIER
Antibodies		
anti-Rad53	abcam	Cat# ab104232; RRID:AB_2687603
Anti-HA 3F10	SIGMA-Aldrich	Cat# 11867423001; RRID:AB_390918
anti-myc 9E10	SIGMA-Aldrich	Cat# 11667149001; RRID:AB_390912
anti-Flag M2	SIGMA-Aldrich	Cat# F3165; RRID:AB_259529
PAP antibody (peroxidase anti-peroxidase)	SIGMA-Aldrich	Cat# P1291; RRID:AB_1079562
anti-mouse IgG HRP sheep	GE Healthcare Lifescience	Cat# 10094724; RRID:AB_772209
Goat anti-rat IgG HRP	Millipore	Cat# AP202P; RRID:AB_805331
Bacterial and Virus Strains		
DH5α	Thermo-Fisher	Cat# 18265017
MC1061	Own lab	N/A
Chemicals, Peptides, and Recombinant Proteins		
Hydroxyurea	SIGMA-Aldrich	Cat# H8627
Methyl methanesulfonate	SIGMA-Aldrich	Cat# 129925
(S)-(+)-Camptothecin	TCI (Tokyo Kasei)	Cat# C1495
alpha factor	GENSCRIPT	Cat# RP01002
l-canavanine	SIGMA-Aldrich	Cat# C9758-250
Acid-washed glass beads	SIGMA-Aldrich	Cat# G8722
Complete EDTA free protease inhibitor cocktail	SIGMA-Aldrich	Cat# 5056489001
Dithiothreitol	SIGMA-Aldrich	Cat# D9163
Blotting paper	GE Healthcare	Cat# 80621129
PVDF Membranes	GE Healthcare	Cat# 10600021
Immobilon Western ECL	Millipore	Cat# WBLKS0500
Agarose low EEO	Condalab	Cat# 8010
β-Mercaptoethanol	BIO-RAD	Cat# 161-0710
Phleomycin	APOLLO	Cat# BI3852
Critical Commercial Assays		
Dynabeads Protein G	Fisher	Cat# 10446293
Experimental Models: Organisms/Strains		
Yeast strains used in this study (W303 and BY4741)	Table S1	N/A
Recombinant DNA		
Plasmids used in this study	Table S1	N/A
Software and Algorithms		
ImageJ	National Institutes of Health, Bethesda, Maryland, USA.	https://imagej.nih.gov/ij/, 1997-2018.
Image Lab	Bio-Rad	https://www.bio-rad.com
bz-rate	Laboratory of Computational and Quantitative Biology, Sorbonne Université	http://www.lcqb.upmc.fr/bzrates
Daniel's XL Toolbox	Daniel Kraus, Würzburg, Germany	https://www.xltoolbox.net
ImageGauge	Fuji	https://www.fujifilm.com

LEAD CONTACT AND MATERIALS AVAILABILITY

Further information and requests for resources and reagents should be directed to and will be fulfilled by the Lead Contact, Jordi Torres-Rosell (jordi.torres@cmb.udl.cat). Plasmids and yeast strains generated in this study are available upon request without restrictions.

EXPERIMENTAL MODEL AND SUBJECT DETAILS

All strains used in this study are derivatives of W303 (*MATa ade2-1 can1-100 his3-11,15 leu2-3,112 trp1-1 ura3-1 RAD5+*) or BY4741 (*MATa his3Δ1 leu2Δ0 met15Δ0 ura3Δ0)*. A list of yeast strains used in this study, together with their relevant genotype, is provided in Table S1. Additionally, a list of yeast strains used in each figure is provided in Table S2. Yeast cells were grown in YP (Yeast extract and Peptone) or synthetic complete (SC) drop-out medium (yeast nitrogen base with all amino acids), plus the indicated carbon source at 2% final concentration. For auxin-induced degrons, IAA (SIGMA) was added to 1 mM from a 0,5 M stock in water.

METHOD DETAILS

Construction of mutants strains and plasmids

Epitope tagging of genes and deletions were performed as described (Janke et al., 2004; Goldstein and McCusker, 1999). Fusion of genes to an auxin-induced degron was done as described (Nishimura et al., 2009).

A list of plasmids used in this study is provided in Table S1. Additionally, plasmids used in each figure is provided in Table S2. The *smc5-KallR* sequence was obtained by gene synthesis (Genscript) and cloned into a yeast expression vector to generate pMB1132. To construct a collection of *smc5-KR* mutants affected in each of the five domains in the protein, we first generated a gap by PCR on the pTR927 plasmid, expressing the wild-type *SMC5* allele. Then, we amplified by PCR the *SMC5* sequence omitted in the gap, plus 40 nucleotide tails, from pMB1132 (containing the *smc5-KallR* mutant allele) to create a donor sequence for subsequent homologous recombinational repair. Both PCR products were treated with DpnI to degrade templates and were co-transformed into *E.coli* MC1061 (*recA+*) cells. For *smc5-KR* mutants affected in the coiled coil domain (Figure 3), we repeated the same strategy, but selectively amplifying wild-type *SMC5* and mutant *smc5-KR* sequences to create the adequate combination of gapped plasmids and donor sequences with homologous flanking regions. In all cases, recombinant products were sequenced to verify mutations. The *smc5-KR13* allele was generated through two rounds of mutagenesis to first target K310 and K311, and then K323 and K327. For integration of *smc5-KR10* and *smc5-KR13* alleles, the full *SMC5* sequence was amplified by PCR and fused to an epitope tag (9xmyc or 6xHA) and a selection marker. Clones were screened by western blot and the presence of the *KR* mutations were confirmed by sequencing.

MMS sensitivity assays

10-fold dilution series of yeast cultures were spotted on solid YPD (Yeast extract, Peptone, 2% Glucose) medium containing the indicated concentrations of methyl methanesulfonate (MMS; SIGMA). Plates were incubated at 30°C until individual colonies became visible in the control without MMS.

Cell cycle experiments

Exponentially growing cells were arrested in G1 by addition of 10^{-8} M alpha factor (Genscript) for *bar1Δ* cells and 10^{-6} M for *BAR1* cells at 30°C for 2 hours or until > 95% of cells were arrested in G1. In Figure 7, G1-arrested cells were treated with 0,01% MMS (SIGMA) for 30 min to induce a pulse of alkylation damage. Cultures were released by washing cells 3 times with pre-warmed medium and re-suspended in media containing 0,1 mg/ml pronase E (SIGMA). DNA was stained using Hoechst at 0,5 μg/ml final concentration in the presence of mounting solution and 0,4% Triton X-100 to permeabilize cells. For fluorescence microscopy, series of z-focal plane images were collected with a DP30 monochrome camera mounted on an upright BX51 Olympus fluorescence microscope.

Pull down analysis of sumoylated proteins

Pull down analysis of sumoylated proteins was performed as previously described (de Bettignies and Johnston, 2003). To purify sumoylated proteins, the budding yeast SUMO gene (*SMT3*) was tagged N-terminally with a 6xHis-Flag epitope. 100 ODs cultures were collected and cells were mechanically broken in 6M guanidine chloride. Protein extracts were incubated with Ni-NTA beads in the presence of 15 mM imidazole overnight at room temperature. Beads were extensively washed with 8 M urea and bound proteins were eluted with SDS-PAGE loading buffer. In all cases, SUMO pull downs were loaded in SDS-PAGE gels next to protein extracts to confirm the slower mobility of SUMO conjugates with respect to the unmodified protein.

Co-immunoprecipitation analysis

For co-immunoprecipitation analysis shown in Figure 4, protein extracts were prepared in EBX as previously described (Almedawar et al., 2012), and incubated with anti-HA beads (Pierce). Beads were then washed 6 times with EBX buffer before elution in loading buffer. Protein extracts for Mph1-TAP and Mhf1-TAP immunoprecipitations shown in Figure 6 were prepared in extract buffer (50mM

TrisHCl pH 7, 5% glycerol, 150 mM NaCl, 0,1% Triton X-100, 0,1 mM DTT, 10 mM NEM) containing protease inhibitors (Roche). 60 ODs of cells were mechanically broken in 250 μL of extract buffer using a bead beater. Protein extracts were incubated with IgG agarose beads (SIGMA). Beads were washed 3 times for 8 minutes in extract buffer, and proteins finally eluted by incubation in 2% SDS for 10 minutes at 37°C. Antibodies used for western blot analysis were anti-HA (3F10, Invitrogen), anti-myc (9E10, Roche) and peroxidase anti-peroxidase for TAP (Sigma). Anti-PCNA (anti-Pol30) was a kind gift from Gemma Bellí.

Western blot analysis of PCNA modification

For PCNA western blot, protein extracts were prepared from 12 ODs of cells collected from exponentially growing cultures. Cells were washed with 20% TCA, resuspended in 200 μL of TCA 20%, and mechanically disrupted with an equal volume of glass beads at room temperature. Extract and cell debris were recovered in a new tube, while beads were washed 2 times with 200 μL of 5% TCA. The first extract plus the two sequential washes were combined into a new tube to make 600 μL of total cell extract in 10% TCA. Extracts were spun 10 minutes at maximum speed, the supernatants were discarded and the pellet resuspended in 200 μL 1xSR (2% SDS in 0,125 M Tris-HCl pH 6,8) plus 100 μL of 1M Tris base, boiled for 3 min and clarified by centrifugation 10 min at maximum speed. 25 μg of protein extracts, quantified by BioRad protein assay, were combined with Laemmli buffer and loaded in each lane. Membranes were probed with polyclonal rabbit anti-Pol30 antibody.

Mass spectrometry for identification of Smc5 sumoylation sites

For co-expression of yeast Smc5, yeast Nse2, and the human SUMO2, E1 and E2 enzymes, BL21 cells were co-transformed with 3 plasmids (Figure S3A), grown at 37°C to A600 = 0,6, and then induced to express heterologous proteins by IPTG addition. Cultures were then incubated for 3-4 h at 30°C and harvested by centrifugation. Cell pellets were equilibrated in Lysis Buffer (20% sucrose, 20 mM Tris pH 8, 1 mM β-mercaptoethanol, 350 mM NaCl, 1 mM PMSF, 0,1% IGEPAL), and cells were disrupted by sonication. Cell debris was removed by centrifugation (40,000 × g). GST-Smc5 was purified with glutathione beads, eluted with GST and samples separated on a 7,5% SDS-PAGE. After Coomassie staining, two slices running immediately above GST-Smc5 were cut from the gel. The gel bands were washed with ammonium bicarbonate and acetonitrile (ACN), reduced with DTT and alkylated with chloroacetamide. Afterward, the samples were digested overnight at 35°C with trypsin (sequence grade, Promega). The resulting peptide mixtures were extracted from the gel matrix with 60% ACN and 5% formic acid (FA), dried-down in a SpeedVac system, and stored at −20°C until the subsequent nanoUPLC-mass spectrometry analysis. The dried-down peptide mixtures were analyzed in a nanoAcquity liquid chromatographer (Waters) coupled to a LTQ-Orbitrap Velos (Thermo Scientific) mass spectrometer. The tryptic digests were resuspended in 1% FA solution and injected for chromatographic separation. Peptides were trapped on a Symmetry C18TM trap column, and were separated using a C18 reverse phase capillary column. Eluted peptides were subjected to electrospray ionization. Both a target and a decoy database were searched to obtain a false discovery rate (FDR), and thus estimate the number of incorrect peptide-spectrum matches that exceed a given threshold. To improve the sensitivity of the database search, Percolator (semi-supervised learning machine) was used to discriminate correct from incorrect peptide spectrum matches.

2D gel analysis of replication intermediates

For G1 synchronization, *MATa* cells were grown to an OD600 of 0,35 in YPAD medium before α-factor (10 μg/mL; Biomedal) synchronization for 180 min. Cells were released from α-factor treatment by washing three times in prewarmed, fresh YPAD medium containing 0,1 mg/mL Pronase E (Sigma) prior to addition of 0,03% MMS. DNA isolation and two dimensional (2D) agarose gel electrophoresis was carried out as described in Wellinger et al. (2003). Replication intermediates were detected by Southern blot analysis and hybridization with specific ^{32}P-labeled DNA probes, matching to nucleotides 452691–453344 on chromosome XII. Signals were quantified using a PhosphorImager (FLA 5100) with ImageGauge software (Fuji). The relative intensity of replication intermediates was normalized to the signal intensity obtained in the 1N-spot (non saturating exposure).

Determination of spontaneous mutation rate and BIR assay

Spontaneous mutation rates were determined from at least 7 independent cultures grown to saturation and properly diluted to obtain around 200 colonies in YPD. A lower dilution was plated on canavanine plates to estimate number of canavanine resistant mutants. The bz-rate web tool was used to calculate mutation rate per cell per division (Gillet-Markowska et al., 2015). The BIR assay was performed essentially as described (Anand et al., 2014).

Chromosome spreads

Exponentially growing cultures (5 ODs) were spheroplasted as previously described (Grubb et al., 2015). After spheroplasting, 5 μl of gently resuspended spheroplasts were pipetted onto a glass slide before sequential addition of 10 μl fixative (3,4% sucrose, 4% paraformaldehyde) and 20 μl of 2% lipsol as detergent. One minute later, 20 μl of fixative was added again in a swirling motion. A pipette tip on its side was used to gently spread the nuclei and slides were air-dried overnight. For immunostaining, spreads were washed with PBS for 10 min in coplin jars and incubated with blocking solution (PBS, 2% milk, 5% BSA). Antibodies were incubated in blocking solution for 1 hour in a humidity chamber; monoclonal rat anti-HA (3F10, Roche) was used at 1:500 dilution to detect Smc5-6HA, followed by a 1:1000 dilution of Alexa488 labeled anti-rat antibody. After air-drying, DAPI was added in mounting media.

For fluorescence microscopy, series of z-focal plane images were collected with a DP30 monochrome camera mounted on an upright BX51 Olympus fluorescence microscope. Images were quantified with ImageJ.

QUANTIFICATION AND STATISTICAL ANALYSIS

Specific information about the statistical tests used, number of replicates (N), and p values (p) are described in Figure legends. p values less than 0,05 were considered significant. One-way ANOVA was used in Figures 2, 4, and 6; statistical significance was determined using a Holm-Bonferroni post hoc test. In Figure 5B, the p value was calculated by the Wilcoxon signed-rank test. Statistical analysis was aided by Daniel's XL Toolbox add-in for Excel, version 7.2.13, by Daniel Kraus, Würzburg, Germany (https://www.xltoolbox.net). Bands in western blots were quantified using Image Lab (BioRad). X-shaped structures were quantified using ImageGauge software (Fuji). Mutation rates per cell division and 95% confidence limits were calculated using the bz-rates web tool (http://www.lcqb.upmc.fr/bzrates). Microscopic images were analyzed and quantified manually using ImageJ.

DATA CODE AND AVAILABILITY

This study did not generate nor analyze datasets or new code.